SYNTHESIS OF COLLOIDAL SILVER PARTICLES WITH DIFFERENT SIZES BY SEEDING APPROACH FOR SURFACE ENHANCED RAMAN SCATTERING (SERS) STUDIES

A THESIS SUBMITTED TO
THE GRADUATE SCHOOL OF NATURAL AND APPLIED SCIENCES
OF
MIDDLE EAST TECHNICAL UNIVERSITY

BY

RUKİYE SANCI

IN PARTIAL FULFILLMENT OF THE REQUIREMENTS
FOR
THE DEGREE OF MASTER OF SCIENCE
IN
CHEMISTRY

SEPTEMBER 2009

Approval of the thesis:

SYNTHESIS OF COLLOIDAL SILVER PARTICLES WITH DIFFERENT SIZES BY SEEDING APPROACH FOR SURFACE ENHANCED RAMAN SCATTERING (SERS) STUDIES

submitted by **RUKİYE SANCI** in a partial fulfillment of the requirements for the degree of **Master of Science in Chemistry Department, Middle East Technical University** by

Prof. Dr. Canan Özgen
Dean, Graduate School of **Natural and Applied Sciences** _____

Prof. Dr. Ahmet M. Önal
Head of Department, **Chemistry** _____

Prof. Dr. Mürvet Volkan
Supervisor, **Chemistry Dept., METU** _____

Examining Committee Members:

Prof. Dr. O. Yavuz Ataman
Chemistry Dept., METU _____

Prof. Dr. Mürvet Volkan
Chemistry Dept., METU _____

Prof. Dr. G. İnci Gökmen
Chemistry Dept., METU _____

Prof. Dr. Ceyhan Kayran
Chemistry Dept., METU _____

Assoc.Prof Dr.Atilla Cihaner
Chemistry Group, Atılım University _____

Date: September 11, 2009

I hereby declare that all information in this document has been obtained and presented in accordance with academic rules and ethical conduct. I also declare that, as required by these rules and conduct, I have fully cited and referenced all materials and results that are not original to this work.

Name, Last name: Rukiye Sancı

Signature

ABSTRACT

SYNTHESIS OF COLLOIDAL SILVER PARTICLES WITH DIFFERENT SIZES BY SEEDING APPROACH FOR SURFACE ENHANCED RAMAN SCATTERING (SERS) STUDIES

Sancı, Rukiye

M.S., Department of Chemistry

Supervisor: Prof. Dr. Mürvet Volkan

September 2009, 54 pages

In this study, silver nanorods and nanospheroids were prepared both in aqueous solution and on the surface of glass slides through seed-mediated growth approach at room temperature and used as a surface enhanced Raman scattering (SERS) substrate. The synthesis of metallic nanorods was started with the production of silver nanospheres as seed utilizing sodium borohydride and trisodium citrate as reducing and capping agents, respectively. These seeds were then added to a growth solution containing additional silver salt, ascorbic acid and cetyltrimethylammonium bromide (CTAB.)

Nanorod preparation conditions were first optimized in solution phase. The plasmon absorption of the formed nanocrystals was monitored by UV-Visible spectrometry. The largest red shift in the longitudinal plasmon resonance absorption of silver nanostructures was tried to be achieved in order to realize the highest electromagnetic enhancement in Raman measurements. The images of the formed nanorods were recorded using field emission scanning electron microscopy (FE-SEM).

The optimized colloidal growth conditions were adopted for the growth of nanorods on the surface of the glass substrate. Sol-gel coated glass slides were used in order to increase the porosity on the surface for an effective seeding process. We reported the development of a novel SERS substrate prepared by growing silver nanorods directly on the surface of glass surface without using any linker molecule.

The SERS performances of the nanorod growth surfaces were evaluated with crystal violet (CV), brilliant cresyl blue (BCB) and benzoic acid (BA). Some modifications such as the increase in the $AgNO_3$ concentration in the growth solution and the addition of hydrocarbons to the growth solution were investigated for the enhancement of the SERS signal. The intense spectra obtained for the model compounds demonstrated the efficiency of the prepared substrate for the SERS enhancement and its potential as a SERS detection probe for chemical and biological analysis.

Keywords: Silver, nanorods, seed-mediated growth technique, solid SERS substrate, benzoic acid, crystal violet, brilliant cresyl blue

ÖZ

YÜZEYDE GÜÇLENDİRİLMİŞ RAMAN SAÇILMASI (SERS) ÇALIŞMALARI İÇİN ÇEKİRDEKLEME YÖNTEMİYLE FARKLI BOYUTLARDA KOLLOİD GÜMÜŞ PARÇACIKLARININ SENTEZİ

Sancı, Rukiye

Yüksek Lisans, Kimya Bölümü

Tez Yöneticisi: Prof. Dr. Mürvet Volkan

Eylül 2009, 54 sayfa

Bu çalışmada, çekirdek ortamlı büyüme yaklaşımıyla hem sulu çözeltide ve hem de cam parçaların yüzeyinde gümüş nanoçubuklar ve nanosferoidler oda sıcaklığında hazırlanmış ve yüzeyde güçlendirilmiş Raman saçılması (SERS) substratı olarak kullanılmıştır. Metalik nanoçubukların sentezi gümüş nanokürelerin sodyum borohidrür ve askorbik asitten sırasıyla indirgeyici ve sınırlandırıcı maddeler olarak faydalanılmasıyla çekirdek olarak üretilmesiyle başlar. Bu çekirdekler daha sonra gümüş tuzu, askorbik asit ve setiltrimetil amonyum bromür (CTAB) içeren büyüme çözeltisine ilave edildi.

Nanoçubuk hazırlama koşulları ilk önce çözelti fazında optimize edildi ve oluşan nanokristallerin plazmon absorpsiyonları UV-Visible spektrometre ile gözlendi. Gümüş nanoyapıların uzunlamasına plazmon resonanslarında kırmızıya doğru en büyük kayma Raman ölçümlerinde en yüksek elektromanyetik güçlendirmeyi elde etmesi için en iyi koşullara getirildi. Oluşturulan nanoçubukların görüntüleri Alan Emisyonlu Taramalı Elektron Mikroskobu (AETEM) kullanılarak kaydedildi.

Optimize edilen kolloid büyüme çözeltisi koşulları nanoçubukların cam substratın yüzeyinden büyümesi için uyarlanmıştır. Etkili bir çekirdekleme işlemi için yüzeydeki pürüzlülüğü artırmak amacıyla sol-jel kaplı cam parçaları kullanıldı. Bu çalışmada hiçbir bağlayıcı molekül kullanmadan cam substratın yüzeyinden büyümüş gümüş nanoçubuklarla hazırlanan SERS yüzeylerinin hazırlanışı sunulmaktadır.

Gerekli nanoyapıların üretilmesi kimyasal indirgenme, kimyasal sıvı toplama, termal toplama, fotokimyasal indirgenme radyolizi gibi çeşitli üretim yöntemlerine dayanmaktadır. Bu çalışmada çekirdek ortamlı büyütme yaklaşımıyla değişik boyuttaki kolloidal Ag parçaların sentezini açıklanmaktadır. Yöntem, çekirdeklenme ve arkasından parçaların büyütülmesi olmak üzere iki aşamalı işlemden oluşmaktadır.

Kolloid nanoparçacıkların ve nanoparçacık tutturulmuş katı yüzeylerin SERS güçlendirme performansları kristal eflatun (KE), parlak kresil mavi (PKM) ve benzoik asit (BA) örnek maddelerle değerlendirilmiştir. Büyüme çözeltisindeki $AgNO_3$ derişiminde artış ve büyüme çözeltisine hidrokarbon ilavesi gibi değişikliklere SERS sinyalinin güçlendirilmesi için bakılmıştır. Örnek bileşenler için elde edilmiş olan güçlü spektralar, SERS güçlendirmesi için hazırlanmış olan substratların yeterliliğini ve kimyasal ve biyolojik analizler için SERS tayin probu gibi çalıştığını gösterir

Anahtar Kelimeler: Gümüş, nanoçubuk, yüzeyde güçlendirilmiş Raman saçılması, katı SERS substratı, benzoik asit, kristal eflatun, parlak kresil mavisi

To My Family

ACKNOWLEDGEMENTS

I wish to express my gratitude to my supervisor Prof. Dr. Mürvet Volkan for her guidance, encouragement, understanding and suggestions throughout this research.

I would like to thank to Assist. Prof. Dr. Bilsen Tural for her patience while doing the very first experiments of this study.

I am deeply grateful to Seher Karabıçak, Murat Kaya and Bahar Köksel for their help, support and friendship.

I would like to thank to all my lab mates in C-50 Analytical Research Group for their friendship.

I want to thank Necati Koç for his help, all AtaMAn Research Group members for their understanding and friendship.

Finally, my special thanks to my mother, father, and sister for their trust, patience, support and love.

TABLE OF CONTENTS

ABSTRACT iv

ÖZ vi

ACKNOWLEDGEMENTS ix

TABLE OF CONTENTS x

LIST OF TABLES xiii

LIST OF FIGURES xiv

CHAPTERS 1

1. INTRODUCTION 1

1.1 Raman Scattering 1
1.2 Surface Enhanced Raman Scattering 5
1.3 Surface Plasmon Absorption 6
1.4 Nanoparticles 9
1.5 Aim of the Study 11
2. EXPERIMENTAL 12

2.1 Chemical and Reagents 12
2.2 Instrumentation 14
2.2.1 Spin Coater 14
2.2.2 Centrifuge 14
2.2.3 UV-Visible Spectrophotometer 14
2.2.4 Surface Enhanced Raman Spectrometer (SERS) 14
2.2.5 Field Emission Scanning Electron Microscopy (FESEM) 14
2.3 Procedures 15
2.3.1 Preparation of Silver Nanorods in the Solution Phase 15
2.3.1.1 Preparation of Seed Solution 15

2.3.1.2 Optimization of the Growth Conditions 15
2.3.1.2.1 The Effect of Equilibrium Molar Concentration of Ascorbic Acid 15
2.3.1.2.2 Ageing Time of Growth Solution 16
2.3.1.2.3 The Effect of Seed Volumes.....16
2.3.1.2.4 The Effect of CTAB Concentration 17
2.3.1.2.5 Repeatability of the Optimized Growth Conditions 17
2.3.1.2.6 Optimization of the Sequence of the Addition of the Reagents ..18
2.3.1.2.7 Characterization of Nanoparticles.....18
2.3.2 Preparation of Solid SERS Substrates 19
2.3.2.1 Coating of Glass Slides by Sol-Gel 19
2.3.2.2 Preparation of the Silver Nanorods on the Solid Substrate Surface ...19
2.3.3 Performance of Synthesized Nanoparticles 20
2.3.3.1 Effect of Silver Nitrate to the Growth Solution for Nanoparticle Attached Solid Substrate 20
2.3.3.2 Effect of Organic Solvents to the Growth Solution for Nanoparticle Attached Solid Substrate 20
2.3.3.3 Effect of Seed Addition to the Growth Solution 20
3. RESULTS AND DISCUSSION 21
3.1 Synthesis of Silver Nanorods.....21
3.1.1 Preparation of the Seed Solution 21
3.1.2 Optimization of the Growth Conditions 22
3.1.2.1 The Effect of Equilibrium Molar Concentration of Ascorbic Acid....22
3.1.3.2 Ageing Time of Growth Solution.....25
3.1.3.3 Seed Volume Optimization 26
3.1.3.4 CTAB Optimization.....32
3.1.3.5 Repeatability of the Optimized Growth Conditions 37
3.1.3.6 Sequence of Addition of Reagents to the Growth Solution 38
3.2 Characterization of Nanoparticles.....39
3.3 Preparation and SERS characterization of glass substrates through seed-mediated growth approach 40
3.3.1 Parameters affecting SERS intensity of nanoparticles attached to the sol-gel coated glass substrate.....41
3.3.1.1 Effect of silver nitrate 42
3.3.1.2 Effect of organic hydrocarbons to the growth solution to prepare nanoparticle attached solid substrate.....43

3.3.1.3 Effect of seed addition to the growth solution to prepare nanoparticle in colloid 46
3.3.1.4 SERS performance of nanoparticle colloid vs SERS performance of nanoparticle attached solid substrate 47
4. CONCLUSIONS 49
REFERENCES 51

LIST OF TABLES

TABLES

Table 3.1 The plasmon bands of growth solution of which absorption profile is given in Figure 3.6.....24

Table 3.2. The change in the wavelength and absorbance of the surface plasmon bands of growth solutions prepared with 0.250 mL and 0.125 mL seed addition with respect to time.....26

Table 3.3 The plasmon bands of growth solution prepared with 0.072 M CTAB, $2.25x10^{-4}$ M $AgNO_3$, $4.50x10^{-3}$ M ascorbic acid, different volumes of seed (2.00, 1.00, 0.500, 0.250, 0.125 and 0.060 mL) and 0.045 M NaOH.....29

Table 3.4 The plasmon bands of growth solution prepared with 0.093 M CTAB, $2.58x10^{-4}$ M $AgNO_3$, $2.58x10^{-3}$ M ascorbic acid, different volumes of seed (2.00, 1.00, 0.500, 0.250, 0.125 and 0.060 mL) and 0.026 M NaOH.....31

Table 3.5 The plasmon bands of growth solution prepared with 7 mL different concentration of CTAB, $3.22x10^{-4}$ M $AgNO_3$, $2.06x10^{-3}$ M ascorbic acid, 0.250 mL seed, and 0.064 M NaOH. 34

Table 3.6 Optimized conditions for colloidal growth solution with the ageing time of 2 h. 35

Table 3.7 The plasmon bands of growth solution prepared with different volumes of 80 mM CTAB (5.00 mL,6.00 mL, 7.00 mL, 8.00 mL, 9.00 mL, 10.00 mL), 0.25 mL of 10 mM $AgNO_3$, 0.25 mL seed and 0.1 mL of 5 M NaOH.....37

LIST OF FIGURES

FIGURES

Figure 1.1 Energy level diagram showing the states involved in Raman signal. The line thickness is roughly proportional to the signal strength from the different transitions [3]. 3

Figure 1.2 Stokes and anti-Stokes Raman spectral lines of CCl_4, excited by the 514.5 nm line of an argon ion laser. The frequency differences between the excitation radiation and the Raman scattered radiation are called the Raman Shift. Raman shifts are reported in units of wavenumber (cm^{-1}) and are defined by: υ (cm^{-1}) = ($1/\lambda_o$-$1/\lambda_R$), where λ is the Raman Shift, λ_o is the laser wavelength, and λ_R is the Raman radiation wavelength [3]. 4

Figure 1.3 Schematic representation of the plasmon resonance in anisotropic particles. *E* is the oscillating electric field of the incident light. For a rodlike particle, two oscillation modes are possible: (a) the transverse oscillation (along the *B* or *C* axis) and (b) the longitudinal oscillation (along the *A* axis). The plasmon oscillation induces a dipole by local, temporary charge separation [15]. 8

Figure 1.4 Cartoon representation of seed-mediated growth for gold and silver nanorods [46]. 11

Figure 3.1 Schematic representation of oxidation of ascorbic acid to dihydroascorbate anion. 23

Figure 3.2 a) Growth solutions prepared with 0.018 M CTAB, $3.2x10^{-4}$ M $AgNO_3$, $2.1x10^{-3}$ M ascorbic acid, different volumes of seed (0.500, 0.250 and 0.125 mL) and 0.064 M NaOH **b)** Growth solutions prepared with 0.017 M CTAB, $3.1x10^{-4}$ M $AgNO_3$, $6.2x10^{-3}$ M ascorbic acid, different volumes of seed (0.5, 0.25 and 0.125mL) and 0.062 M NaOH.....24

Figure 3.3 UV-visible absorption profile of growth solution prepared with 0.072 M CTAB, $2.25x10^{-4}$ M $AgNO_3$, $4.5x10^{-3}$ M ascorbic acid, different volumes of seed (2.00, 1.00, 0.500, 0.250, 0.125 and 0.060 mL) and 0.045 M NaOH.....28

Figure 3.4 UV-visible absorption profile of growth solution prepared with 0.093 M CTAB, $2.58x10^{-4}$ M $AgNO_3$, $2.58x10^{-3}$ M ascorbic acid, different volumes of seed (2.00, 1.00, 0.500, 0.250, 0.125 and 0.06 mL) and 0.026 M NaOH.....30

Figure 3.5 Cartoon illustrating the formation of the bilayer of C_nTAB (squiggles) on the nanorod (black rectangle) surface may assist nanorod formation as more metal ions (black dots) are introduced [63]. 33

Figure 3.6 UV-visible absorption profile of growth solution prepared with 7 mL of different concentration of CTAB, $3.22*10^{-4}$ M $AgNO_3$, $2.06*10^{-3}$ M ascorbic acid, 0.250 mL seed, and 0.064 M NaOH. 34

Figure 3.7 UV-visible absorption profile of growth solution prepared with 80 mM different volumes of CTAB (5.00 mL,6.00 mL, 7.00 mL, 8.00 mL, 9.00 mL, 10.00 mL) 0.25 mL 10 mM $AgNO_3$, 0.25 mL seed and 0.10 mL 5 M NaOH. AA: ascorbic acid.....36

Figure 3.8 The growth solutions prepared in the same way in the same day. The solution containes $1.8*10^{-2}$ M CTAB, $3.22*10^{-4}$ M $AgNO_3$, $2.06*10^{-3}$ M ascorbic acid, 0.250 mL seed, $6.4*10^{-2}$ M NaOH. 38

Figure 3.9 UV-visible absorption profile of growth solution prepared with "stock growth solution" with 0.1 mL of 1 M NaOH solution.....39

Figure 3.10 The field emission-scanning electron microscopy image of the nanostructures prepared by the growth solution containing 0.12 mL seed solution ..40

Figure 3.11 .The variation of the relative SERS intensities of 10^{-6} M BCB collected on the solid substrates prepared by (A) 3 and (B) 5 fold greater Ag^+ concentration than the optimized growth solution 43

Figure 3.12 The variation of the relative SERS intensities of $1.0x10^{-6}$ M CV collected on the solid substrates prepared by growth solution in the absence (lower trace) and in the presence (upper trace) of 0.36 mL of pure acetone 44

Figure 3.13. The variation of the relative SERS intensities of $1.0x10^{-6}$ M CV collected on the solid substrates prepared by growth solution in the absence (lower trace) and in the presence (upper trace) of 0.27 mL cyclohexane. 45

Figure 3.14 The variation of the relative SERS intensities of BA (10^{-2} M) collected with growth solutions prepared by (A) the addition of 0.125 mL seed solution; (B) the addition of 0.25 mL seed solution. 46

Figure 3.15 The UV-VIS spectra of silver nanorod colloids prepared by (A) the addition of 0.125 mL seed solution ; (B) the addition of 0.25 mL seed solution ; (C) the addition of 0.5 mL seed solution to the growth solutions. 47

Figure 3.16 The SERS spectra of 10^{-2} M BA acquired with the silver nanorods colloid solution (A) and silver nanorod coated solid substrate (B). 48

CHAPTER 1

INTRODUCTION

1.1 Raman Scattering

Raman spectroscopy is an important mode of gaining information about molecules based upon the scattering of monochromatic light [1]. It has served as a valuable tool in the characterization of compounds due to the structural information that it provides. Due to its narrow spectral lines, Raman spectroscopy could enable the analyses of multicomponent samples without complicated separation procedures. This feature would be particularly useful for in situ monitoring of complex environmental samples [2].

The Raman effect arises when a beam of intense monochromatic radiation passes through a sample that contains molecules undergoing a change in molecular polarizability as they vibrate. Recall that in order for a vibrational mode to be active in the infrared region, the vibration must cause a change in the permanent dipole moment of the molecule [3].

When monochromatic radiation is scattered by molecules, a small fraction of the scattered radiation is observed to have a different frequency from that of the incident radiation; this is known as the Raman effect and the wavelengths are called Raman wavelengths [3]. Each of these is shifted from the incident wavelength by an amount that corresponds to the energy involved in a change in vibration or another characteristic motion for an analyte. The collection of such lines for a particular species is simply its Raman spectrum [1]

Since its discovery in 1928, the Raman effect has been an important method for the elucidation of molecular structure, for locating various functional groups or chemical bonds in molecules, and for the quantitative analysis of complex mixtures, particularly major components. Although vibrational Raman spectra are related to infrared absorption spectra, a Raman spectrum arises in a different manner and thus often provides the complementary information. Vibrations that are active in Raman scattering may be inactive in the infrared, and vice versa. A unique feature of Raman scattering is that each line has a characteristic polarization, and polarization data provide additional information about molecular structure [1].

Most collisions of the incident photons with the sample molecules are elastic (Rayleigh scattering). The electric field produced by the polarized molecule oscillates at the same frequency as the passing electromagnetic wave so that the molecule acts as a source sending out radiation of that frequency in all directions. As shown in Figure 1.1, the incident radiation does not raise the molecule to any particular quantized level; rather, the molecule is considered to be in a virtual excited state. As the electromagnetic wave passes, the polarized molecule ceases to oscillate and returns to its original ground level in a very short time (approximately 10^{-12} s.).

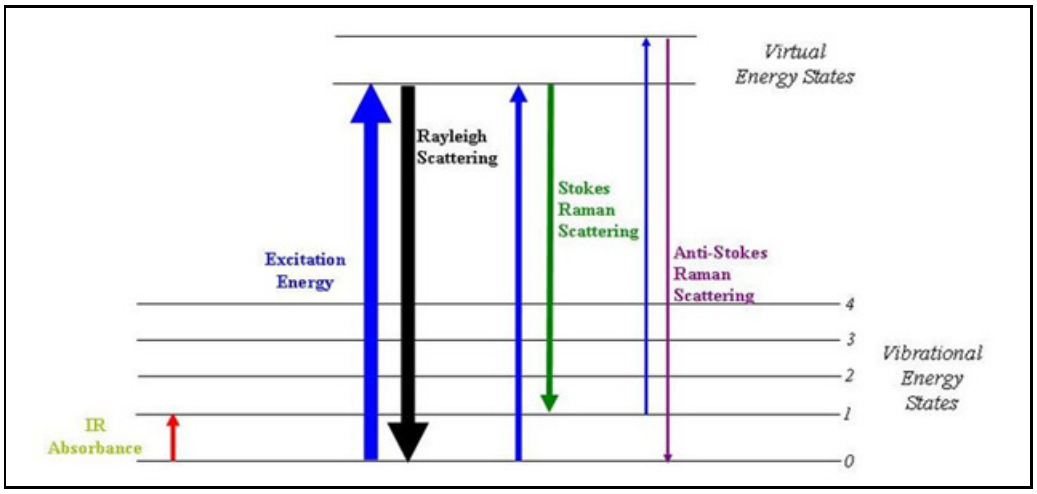

Figure 1.1 Energy level diagram showing the states involved in Raman signal. The line thickness is roughly proportional to the signal strength from the different transitions [3].

Usually incident radiation, ν_0, is absorbed by a molecule in the lowest vibrational state. If the molecule reemits by returning not to the original vibrational state, but to an excited vibrational level, ν_v, of the ground electronic state, the emitted radiation is of lower energy-that is, lower frequency ($\nu_0 - \nu_v$) than the incident radiation. The difference in frequency is equal to a natural vibration frequency of the molecule's ground state. Several such shifted lines (the Stokes lines) normally are observed in the Raman spectrum, corresponding to the different vibrations in the molecule. This provides a richly detailed vibrational spectrum of a molecule (Figure 1.2).

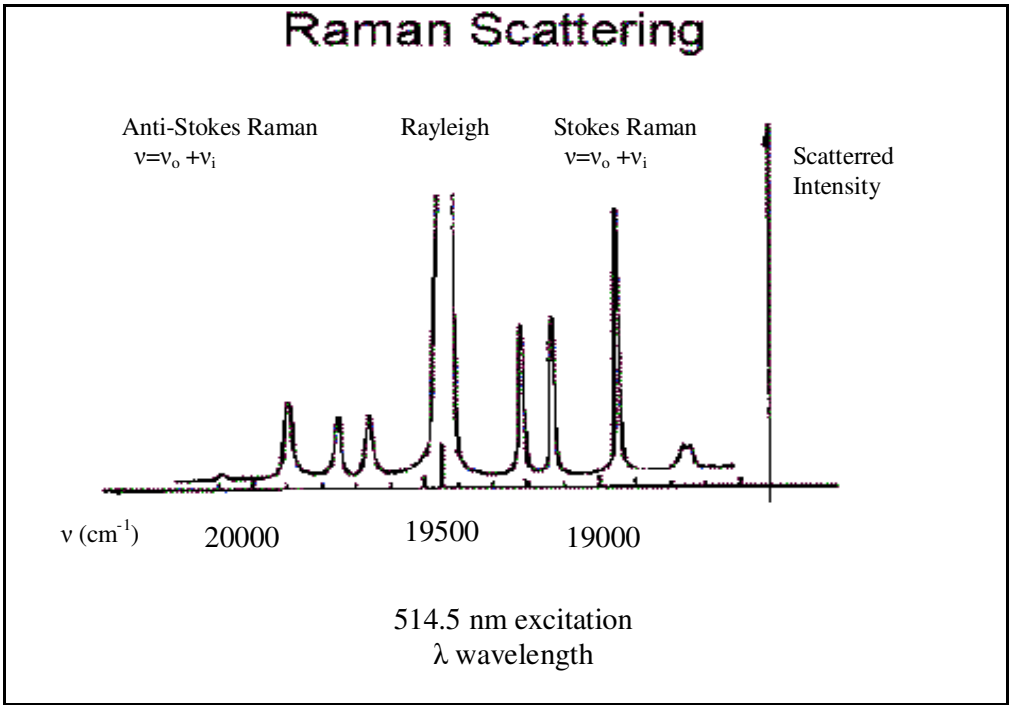

Figure 1.2 Stokes and anti-Stokes Raman spectral lines of CCl_4, excited by the 514.5 nm line of an argon ion laser. The frequency differences between the excitation radiation and the Raman scattered radiation are called the Raman Shift. Raman shifts are reported in units of wavenumber (cm^{-1}) and are defined by: υ (cm^{-1}) = ($1/\lambda_o$-$1/\lambda_R$), where λ is the Raman Shift, λ_o is the laser wavelength, and λ_R is the Raman radiation wavelength [3].

A few of the molecules initially absorb radiation while they are in an excited vibrational state and decay to a lower energy level, so that the Raman frequency is higher than the incident radiation. These are the anti-Stokes lines. Thus the spectrum of the scattered radiation consists of a relatively strong component with frequency unshifted (Rayleigh scattering) corresponding to photons scattered without energy exchange, and the two components of the Raman spectrum: the Stokes lines and the anti-Stokes lines. Normally only the Stokes lines are considered in chemical analysis. These are more intense because, under real circumstances, most molecules are initially in the lowest vibrational level [3].

In the usual Raman method the excitation frequency of Raman sources is selected to lie below most $S \rightarrow S^*$ electronic transitions and above most fundamental vibrational frequencies, but this need not be the case [3].

1.2 Surface Enhanced Raman Scattering

A great disadvantage in any application of Raman spectroscopy results from the extremely small cross section of the Raman process, which is 12–14 orders of magnitude below fluorescence cross sections. Raman cross sections are between 10^{-31} and 10^{-29} cm^2/molecule; the larger values occur only for resonance Raman scattering. Fluorescence cross sections are determined by the product of the absorption cross section and fluorescence quantum yield. They can reach 10^{-16} cm^2/molecule. In SERS, molecules are attached to a metallic 'nanostructure' [4].

The detection limits in spontaneous Raman scattering are on the order of 10^{-1} M concentrations, i.e. orders of magnitude higher than physiologically relevant values. The detection limits could be decreased by many orders of magnitude by exploiting the SERS effect [4].

The importance of SERS is that the surface selectivity and sensitivity extends Raman scattering utility to a wide variety of interfacial systems previously inaccessible to Raman scattering because Raman scattering is not surface sensitive [5].

The enhancement effect can affect either (i) the molecular polarizability (i.e., molecular effect) or (ii) the electric field experienced by the molecule (i.e., field effect). Several enhancement processes may also occur simultaneously. As a result, theoretical models generally involve two major types of enhancement mechanisms: (1) an `electromagnetic effect' (sometimes referred to as the field effect) in which the molecule experiences large local fields caused by electromagnetic resonances occurring near metal surface structures, and (2) a `chemical effect' (also referred to as the molecular effect) in which the molecular polarizability is affected by interactions between the molecule and the metal surface [6].

Raman scattering is enhanced when the analyte is absorbed on colloidal metallic surfaces. Silver, gold, and copper are the metals found to be most effective. For colloidal silver particles, the enhancement factors are typically 10^{-3}-10^{-6} times the normal Raman intensities. Surface enhancement and resonance enhancement effects are multiplicative, thus leading to large Raman signals and low detection limits, often in the range of 10^{-9}-10^{-12} [7].

1.3 Surface Plasmon Absorption

In noble metals, the decrease in size below the electron mean free path (the distance the electron travels between scattering collisions within the lattice centers) gives rise to intense absorption in the visible region of the electromagnetic spectrum [8]. This results from the collective excitation of electrons in the conduction band of nobel metal nanoparticles arising from resonance with incident visible radiation is referred to as localized surface plasmon resonance (LSPR) and is responsible for this strong absorption in visible region [9].

Mie Theory [10] has been used to calculate the spectra of particles smaller than the wavelength of light for nanoparticles whose metallic dielectric function is known and which are embedded in an environment of known dielectric constant [6,8,9] .

The optical response of spherical Ag nanoparticles exhibits a single absorption band attributed to the collective dipole oscillation (surface plasma resonance). However, it usually deviates from this single-band spectral feature while modifying the shape and size of the particles. For example, the classical electrostatic model predictions of absorption cross sections for nanospheroids of both gold and silver have been demonstrated to split the dipolar resonance into two surface plasmon bands [9].

The shape dependence of the surface plasmon absorption can be modeled using the Gans Theory [11] which is an extension of the Mie Theory [10] with a geometrical factor. This theory demonstrates that for elongated ellipsoids the direction of the plasmon oscillation depends on the orientation of the particle axis with respect to the

wavevector of incident light as shown in Figure 1.3. Two absorption bands are shown: one is due to the coherent electronic oscillation along the short axis (the transverse absorption band), and the other (the longitudinal band) is at a longer wavelength, which is more intense and results from the coherent electronic oscillation along the long axis. The absorption maximum of the latter band is sensitive to the rod length [8]. Aspect ratio is defined as the ratio of long axis to short axis or in other words ratio of length L over diameter d [8]. The Gans Theory predicts that the longitudinal resonance shifts to longer wavelengths with increasing aspect ratio, whereas the transverse resonance shifts to slightly shorter wavelengths [12-15].

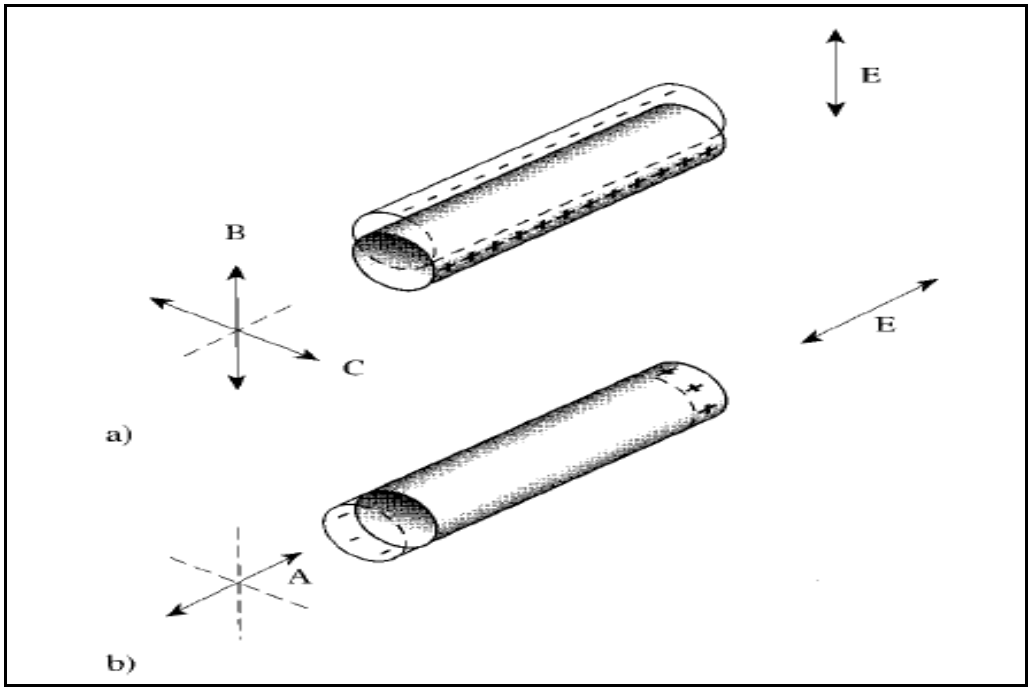

Figure 1.3 Schematic representation of the plasmon resonance in anisotropic particles. *E* is the oscillating electric field of the incident light. For a rodlike particle, two oscillation modes are possible: (a) the transverse oscillation (along the *B* or *C* axis) and (b) the longitudinal oscillation (along the *A* axis). The plasmon oscillation induces a dipole by local, temporary charge separation [15].

Application of surface plasmon resonance has occured in sensor technology, in the characterization of molecules at a dielectric-metal interface [16], in extremely sensitive SERS [17] and in plasmonic devices [18].

Recently, subwavelength transport of surface plasmons was demonstrated [19] and there has been intensive interest in the properties of surface plasmons in confined metal structures [20-25]. As for the observation of electromagnetic (EM) enhancement from nanostructures at scales below 100 nm, explanations for the observed enhancement factors in SERS and the spatial distribution of the electric

field near the metal nanorod, as well as the role played by the plasmon modes in the rod, are still not fully understood.

1.4 Nanoparticles

A transition from the bulk band structure to individual localized energy levels occurs in clusters of subnanometer to nanometer size, and the detection of quantum size effects has been of great interest to scientists in the search for novel materials with exciting new properties [26].

Because bulk silver exhibits the highest electrical and thermal conductivities among all metals, it seems to be interesting and fruitful to synthesize and study silver nanorods. Silver has also been extensively exploited in a variety of applications that range from catalysis, through electronics, to photonics and photography. The performance of silver in most of these applications could be significantly enhanced by processing silver into rod-like nanostructures with well-controlled dimensions [27].

Synthesis of metal nanostructures has been an active research area for many decades, because of the importance of these materials to catalysts [28], photocatalysts [29], sensors [30] and ferrofluids [31] and because of their applications in optoelectronics [32] and in electronic [32] and magnetic [30] devices.

Synthesis of nanorods can be divided into following groups:

Synthesis in hard templates: In this approach, hard templates require subsequent steps in which the solid template has to be replaced by a liquid in order to obtain a dispersion. The advantage of hard templates is that it allows for easy adjustment of the length. Furthermore, the pore diameter can be increased by slow dissolution of the hard template, enabling the preparation of rods with different sizes but the same aspect ratio [13,16, 33-40].

Synthesis with soft templates: Rodlike micelles, microemulsions, and surfactants in solution can also direct the growth of anisotropic nanomaterials. The shape of the rodlike micelle promotes the formation of rodlike nanomaterials from ionic precursors; in the case of surfactants, "medium-strength" binding of a surfactant to a growing crystal face helps direct nanorod growth. The aspect ratio of the resulting nanorods can be controlled by the shape and size of the micellar/microemulsion template, and by the relative concentrations of precursors, salts, and surfactants [41-45].

Seed-Mediated growth in solution: Murphy and co-workers developed a seed-mediated growth approach to making metallic nanorods in aqueous solution at or near room temperature [46-57].

The procedure shown in (Figure 1.4) begins with the synthesis of metallic nanospheres by chemical reduction of a metal salt with a strong reducing agent such as sodium borohydride, and in the presence of trisodium citrate as capping agent to stabilize the nanoparticles and to prevent particle growth. The preformed silver spheres serve as seeds on which to grow more anisotropic nanostructures. These seeds are then added to a solution containing additional silver salt to promote silver growth in solution by chemical reduction of silver salt, a weak reducing agent (e.g., ascorbic acid), and a rodlike micellar template (cetyltrimethylammonium bromide, CTAB). The seeds serve as nucleation sites for nanorod growth. Moreover, NaOH is added to arrange the pH of the solution [46].

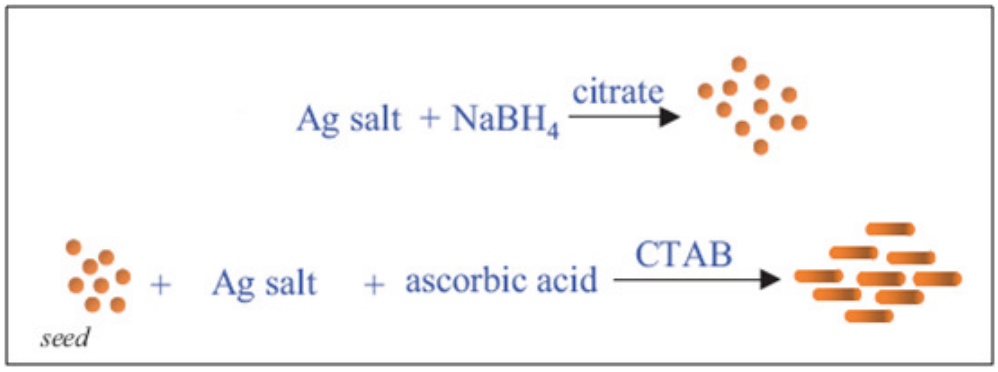

Figure 1.4 Cartoon representation of seed-mediated growth for gold and silver nanorods [46].

1.5 Aim of the Study

In this study, silver nanorods with seed mediated growth approach were synthesized in colloidal solutions and also on solid glass substrates. The surface plasmon resonances of colloidal silver solutions were followed by UV-Visible spectrophotometry. Field Emission Scanning Electron Microscopy (FE-SEM) in METU Central Laboratory was used for their characterization. These nanoparticles, both in the solution phase and on the glass surface, were used as SERS substrates for the detection of model compounds such as benzoic acid, brilliant cresyl blue and crystal violet.

CHAPTER 2

EXPERIMENTAL

2.1 Chemical and Reagents

i) Silver nitrate ($AgNO_3$), has been purchased from Merck KGaA Darmstadt, Germany.

ii) Trisodium Citrate ($Na_3C_6H_5O_7$), has been used as capping agent in seed solution, acquired from Fisher Scientific, Leicestershire.

iii) Sodium borohydride ($NaBH_4$), has been used as reducing agent in seed solution and purchased from Merck KGaA Darmstadt, Germany.

iv)Hexadecyltrimethylammoniumbromide ($CH_3(CH_2)_{15}N(Br)(CH_3)_3$) (CTAB), has been used as template of the growth solution and purchased from Aldrich,

v) Ascorbic acid ($C_6H_8O_6$), has been used as reducing agent in growth solution and purchased from Aldrich

vi) Sodium hydroxide (NaOH), has been used for the preparation of pH ~11 template solution and purchased from Fisher Scientific, Leicestershire.

vii) Tetraethoxysilane ($SiC_8H_{20}O_4$) (TEOS), has been purchased from Merck KGaA Darmstadt, Germany.

viii) Methyltriethoxysilane ($C_7H_{18}O_3Si$) (MTEOS), has been purchased from Fluka.

ix) Ethanol (C_2H_5OH), has been purchased from Merck KGaA Darmstadt, Germany

x) Acetone (**C_2H_6O),** has been purchased from J. T. Baker

xi) Concentrated Nitric acid, 36% (w/w), has been purchased from J. T. Baker,

xii) Benzoic Acid (BA), has been purchased from Merck KGaA Darmstadt, Germany

xiii) Brilliant Cresyl Blue (BCB), has been purchased from Aldrich

xiv) Crystal Violet (CV), has been purchased from Aldrich

The microscope slide was ordered from Sail Brand (size: 25.4 mm x 76.2 mm x 1.2 mm). In the preparation of the solutions, deionized water (Millipore, Ltd. resistivity > 18 MΩ) was used.

All other reagents were of analytical-reagent grade. De-ionized water obtained from a Millipore water purification system was used for sample and standard preparations. All the glassware and plastic ware were cleaned by soaking them in 10 % HNO_3 for at least 24 h and then rinsing three times with distilled water and with deionized water.

To measure the pH of the prepared colloidal growth solutions pH paper was used. The catalog number is 1.09535.0001 which was purchased from Merck KGaA Darmstadt, Germany

2.2 Instrumentation

2.2.1 Spin Coater

For spin coating of sol-gel to the substrate, Spincoat G3-8 was purchased from Specialty Coating Systems, Inc.

2.2.2 Centrifuge

Sigma 2-16 model centrifuge was used to separate nanorods from nanospheres.

2.2.3 UV-Visible Spectrophotometer

To follow the optical properties of the nanoparticles, Cary 100 Bio UV-Visible spectrophotometer was used.

2.2.4 Surface Enhanced Raman Spectrometer (SERS)

SERS-active measurements were performed with Jobin Yvon LabRam confocal microscopy Raman spectrometer with a charge-coupled device (CCD) detector and a holographic notch filter. The spectrograph was equipped with a 1800-grooves/mm grating and all measurements were performed with a 200-μm entrance slit. SERS excitation was provided by 632.8-nm radiation from a He-Ne laser with a total power of 20 mW.

2.2.5 Field Emission Scanning Electron Microscopy (FESEM)

For substrate characterization, FEI Quanta 400 F (FE-SEM) was operated at 30 kV at high vacuum at METU Central Laboratory.

2.3 Procedures

2.3.1 Preparation of Silver Nanorods in the Solution Phase

We prepared borohydride-reduced silver nanoparticle seeds and mixed them with a growth solution containing silver salt, a miceller template, ascorbic acid and sodium hydroxide.

2.3.1.1 Preparation of Seed Solution

A seed solution of Ag colloid was prepared by the addition of 0.60 mL of ice cold aqueous solution of 0.010 M $NaBH_4$ into 20 mL of aqueous solution containing 0.25 mM $AgNO_3$ and 0.25 mM trisodium citrate and the mixture was stirred for 2 h This seed was used 2 h after preparation. But, as stated in the literature [58], if it stays more than 5 h a thin film of particles appeared at the water surface. So it can not be used anymore.

2.3.1.2 Optimization of the Growth Conditions

Growth solution is composed of CTAB, silver nitrate, silver seed, ascorbic acid and NaOH. The concentration of ascorbic acid, NaOH, CTAB, aging time of growth solution and the sequence of addition of the chemicals were optimized to obtain high aspect ratio nanorods giving more red shift in spectrum of UV-Visible Spectrophotometer.

2.3.1.2.1 The Effect of Equilibrium Molar Concentration of Ascorbic Acid

Two different sets of experiments were prepared for these optimizations. In ‘Set 1’, 0.16 mL of 100 mM ascorbic acid and in ‘Set 2’, 0.50 mL of 100 mM ascorbic acid solution were added to the growth solution.

Initially 7 mL of 20 mM CTAB was mixed with 0.125 mL of 20 mM $AgNO_3$ and 0.125 mL H_2O. Then to 'Set 1' 0.16 mL of 100 mM ascorbic acid and to 'Set 2' 0.5 mL of 100 mM ascorbic acid solutions were added to this mixture and mixed. Next a different volumes of seed solution (0.5 mL, 0.25 mL, 0.125 mL) and finally 0.1 mL of 5 M NaOH solution were added. The surface plasmon bands were followed by UV-Visible spectrophotometer .

2.3.1.2.2 Ageing Time of Growth Solution

For this optimization seven different growth solutions in terms of seed solution addition were prepared. Initially 18 mL of 0.1 M CTAB was mixed with 0.25 mL of 20 mM $AgNO_3$ and 0.25 mL H_20. Then, 0.16 mL of 100 mM ascorbic acid was added to this mixture and mixed. Next, different volumes of seed solution (2 mL, 1 mL,0.5 mL, 0.25 mL, 0.125 mL, 0.06 mL, 0.03 mL) and finally 0.5 mL of 1 M NaOH solution were added. The surface plasmon bands were followed by UV-Visible spectrofotometer with respect to time.

2.3.1.2.3 The Effect of Seed Volumes

For this optimization two procedures were followed. One was prepared with 10 mL of 80 mM CTAB, the other was prepared with 18 mL of 100 mM CTAB.

Initially, 10 mL of 80 mM CTAB were mixed with 0.125 mL of 20 mM $AgNO_3$ and 0.125 mL H_20. Then 0.50 mL of 100mM ascorbic acid was added to this mixture and mixed. Next different volumes of seed solution was added (2 mL, 1 mL,0.5 mL, 0.25 mL, 0.125 mL, 0.06 mL) and finally 0.1 mL of 5 M NaOH solution was added. The surface plasmon bands were followed by UV-Visible spectrophotometer with respect to time.

Initially, 18 mL of 100 mM CTAB was mixed with 0.25 mL of 20 mM $AgNO_3$ and 0.25 mL H_20. Then 0.50 mL of 100mM ascorbic acid was added to this mixture and mixed. Next a varied amount of seed solution (2 mL, 1 mL,0.5 mL, 0.25 mL, 0.125

mL, 0.06 mL) and finally 0.1 mL of 5 M NaOH solution were added. The surface plasmon bands were followed by UV-Visible spectrophotometer.

2.3.1.2.4 The Effect of CTAB Concentration

Initially 7 mL CTAB with various concentrations (20 mM, 40 mM, 60 mM and 80 mM) was mixed with 0.125 mL of 20 mM $AgNO_3$ and 0.125 mL H_2O. Then 0.16 mL of 100 mM ascorbic acid was added to this mixture and mixed. Next, 0.25 mL of seed solution and finally 0.1 mL of 5 M freshly prepared NaOH solution were added. The surface plasmon bands were followed by UV-Visible spectrophotometer with respect to time.

At the end to confirm the results one more time in overall we made an experiment with 80 mM CTAB with different volumes. Initially, 80 mM CTAB with various volumes (10 mL, 9 mL, 8 mL, 7 mL, 6 mL and 5 mL) was mixed with 0.125 mL of 20 mM $AgNO_3$ and 0.125 mL H_2O. Then 0.16 mL of 100 mM ascorbic acid was added to this mixture and mixed. Next, 0.25 mL of seed solution and finally 0.1 mL of freshly prepared 5 M NaOH solution were added. The surface plasmon bands were followed by UV-Visible spectrophotometer with respect to time.

2.3.1.2.5 Repeatability of the Optimized Growth Conditions

7 mL of 0.02 M CTAB, 0.25 mL of 10 mM $AgNO_3$, 0.16 mL of 0.10 M ascorbic acid and 0.25 mL seed solution and 0.1 mL of 5.0 M NaOH solution were mixed to make growth solution at the optimized concentrations. This procedure was prepared in three times in the same day to obtain the repeatability. The solution was allowed to stand for 2 h. UV-VIS measurements of the growth solution were performed directly at the end of the aging period.

2.3.1.2.6 Optimization of the Sequence of the Addition of the Reagents

The growth solution was prepared by dissolving 0.02189 g of solid $AgNO_3$ and 6 g of solid CTAB in 200 mL deionized water. The concentration of $AgNO_3$ and CTAB were $6.43x10^{-4}$ M and 0.08 M, respectively. The mixture was heated until the solution became clear. The solution was cooled to room temperature and used as a " stock growth solution". Then 0.16 mL of 100 mM ascorbic acid, 0.25 mL seed solution and 0.1 mL of 1 M NaOH were added to a volume of 7.25 mL "stock growth solution" which is equal to the sum of the volume of surfactant and precursor.

2.3.1.2.7 Characterization of Nanoparticles

For characterization, FE-SEM was used. The surfactant was a very big problem. The excess surfactant should be removed from media to get a clear FE-SEM image. So, a procedure was applied to remove excess surfactant from the nanoparticles. Centrifugation is one of the most used techniques to remove surfactant from the media [44]. The centrifugation speed and time were the two important parameters that were optimized and they were confirmed by FE-SEM images.

This centrifugation procedure was applied to the colloid solutions which were prepared by one-by-one addition. 4.0 mL of the growth solution was centrifuged at a speed of 5000 rpm for 30 minutes to precipitate the nanorods and nanospheroids, then the supernatant was removed and the residue was redispersed in 1.5 mL of deionized water and centrifuged again. This process was repeated three times. Afterwards, 50 μL of the centrifugate was dropped onto carbon coated sample holders, dried and measured by FESEM.

This centrifugation procedure was applied to the colloid solutions which were prepared via "stock growth solution". 7.0 mL of the growth solution was centrifuged at a speed of 6000 rpm for 30 minutes to precipitate the nanorods and nanospheroids, then the supernatant was removed and the centrifuge tube was filled with deionized water and centrifuged again at 6000 rpm for 30 min. The supernatant was removed and the nanoparticles were once more centrifuged after completing with deionized

water. The residue was redispersed in 0.5 mL of deionized water. Afterwards, the carbon coated sample holders were covered with centrifugate, dried and measured.

2.3.2 Preparation of Solid SERS Substrates

2.3.2.1 Coating of Glass Slides by Sol-Gel

The microscope slide was cut into eight pieces and used after being washed in acetone, ethanol, and pure water through sonication and dried at room temperature. The sol was prepared by mixing 1.3 mL of tetraethoxysilane (TEOS), 0.3 mL of methyltiethoxysilane (MTEOS), 5.3 mL of ethanol, 0.8 mL of deionized water and 0.03 mL of concentrated HNO_3. At the end of the exothermic reaction (approximately 1 h), 50 μL of the sol was delivered onto the surface of the glass plate (12.7 mm x 10.0 mm) with care to make sure that the whole surface of the glass was covered. The glass plate was then spun at 2000 rpm for 30 s using a spincoater in order to spread the composite on the glass surface uniformly. The coated glasses were then dried overnight at 40 °C.

2.3.2.2 Preparation of the Silver Nanorods on the Solid Substrate Surface

A piece of sol-gel coated microscope slide was then immersed into the seed solution (given in 2.3.2.1) and left for 2 h to allow the attachment of the Ag seed particles to the surface. Then the microscope slide was removed from the seed solution, washed several times with deionized water and dried at room temperature.

Seed coated slide was immersed in the growth solution and left for 24 h for the formation of nanorods on the surface. Then it was removed from the growth solution, washed several times with deionized water to remove the excess detergent and dried at ambient temperature. Thus, prepared slides were used as a SERS substrate. The growth solution is the modified form of the growth solution which is used in solution phase nanoparticle synthesis : 2 mL of 10 mM $AgNO_3$, 4 mL of 0.10 M ascorbic acid

aqueous solutions were introduced into 7 mL of 0.1 M CTAB and finally the pH of the medium was set to 11 with NaOH.

2.3.3 Performance of Synthesized Nanoparticles

2.3.3.1 Effect of Silver Nitrate to the Growth Solution for Nanoparticle Attached Solid Substrate

Initially 18 mL of 100 mM CTAB was mixed with 2.5 mL of 10 mM $AgNO_3$ for 3 fold and 5.0 mL of 10 mM $AgNO_3$ for 5 fold greater silver concentration. Then, 0.32 mL of 100 mM ascorbic acid and finally 0.2 mL of 1 M NaOH solution was added. The solid substrate, immersed in seed solution for 2 h, was immersed in this growth solution and kept inside for 24 h. Then, the SERS performance was investigated.

2.3.3.2 Effect of Organic Solvents to the Growth Solution for Nanoparticle Attached Solid Substrate

In this study the effect of acetone and cyclohexane addition were investigated on the SERS activity of the solid substrates. 0.36 mL acetone and 0.27 mL cyclohexane were added separately to the growth solutions which were prepared for the formation of nanoparticles attached to the solid substrates. The SERS spectra of CV and BCB were recorded using these substrates.

2.3.3.3 Effect of Seed Addition to the Growth Solution

The growth solutions prepared with 0.125 mL and 0.250 mL of seed addition were also investigated by SERS. Initially, 7 mL of 20 mM CTAB was mixed with 0.125 mL of 20 mM $AgNO_3$ and 0.125 mL H_2O. Then, 0.16 mL of 100 mM ascorbic acid was added to this mixture and mixed. Next, different volumes of seed solution (0.5 mL, 0.25 mL, 0.125 mL) and finally 0.1 mL of 5 M NaOH solution were added. The surface plasmon bands were followed by UV-Visible spectrophotometer.

CHAPTER 3

RESULTS AND DISCUSSION

In order to obtain high aspect ratio nanorods parameters such as the concentration of the NaOH, silver seed, silver nitrate, CTAB and ascorbic acid were optimized. The change in the aspect ratio of the nanoparticles were followed by measuring their plasmon absorptions using UV-Visible spectrometer. Characterization of the particles were done using field emission scanning electron microscopy (FESEM). SERS studies were done using benzoic acid (BA), brilliant cresyl blue (BCB) and crystal violet (CV) as model compounds.

3.1 Synthesis of Silver Nanorods

3.1.1 Preparation of the Seed Solution

Preparation of the silver seeds were done according to the Brust method that uses a strong reducing agent sodium borohydride in the presence of trisodium citrate. Clear yellow sols having plasmon absorption bands in the range of 380-430 nm were obtained. As it is known citrate acts both as a reducing agent and as a capping agent [59]. But due to its weak reducing character, the average size of the particles are relatively large when it is used alone. As a capping reagent, on the other hand, citrate exerts a drastic effect on the size and size distribution of the silver particles that are formed under constant Ag^+ concentration and constant rate of reduction [59].

3.1.2 Optimization of the Growth Conditions

3.1.2.1 The Effect of Equilibrium Molar Concentration of Ascorbic Acid

Ascorbic acid was used as the reducing agent for silver ions. At the beginning of our studies we could not manage to obtain the longitudinal surface plasmon resonance bands even in the presence of different amounts of silver seed at pH values lower than 10. However, when the pH of the solution was increased by adding NaOH to higher pH values, the plasmon bands started to appear. This fact is explained by the increase in reducing power of ascorbic acid in basic solutions [60]. For the nanorod preparation using seed mediated growth approach, it is advised to keep the pH of the growth solution to be higher than the p*K*a of the second proton of ascorbic acid. Which means that the ascorbate dianion is a significant component of the solution [47]. To shift the pH of the solution to the suggested value (≈ 11.8), 0.1 mL of 5 M NaOH was added to the growth solution and the pH of the growth solution was simply controlled by a pH paper.

The reduced and oxidized forms of ascorbic acid is shown in Figure 3.1. Ascorbic acid gives two electrons and silver ion receives one electron. Therefore, stochiometrically, ascorbic acid concentration corresponding o the half of the concentration of the silver ions in the growth solution should be enough for a complete reduction. In these studies almost 10 and 20 fold larger concentrations of ascorbic acid compared to that of silver nitrate were used. The colors of the growth solutions prepared at the stated conditions are shown in Figure 3.2, together with their absorption spectra. The wavelengths of the longitudinal and transverse plasmon bands at their maximum and the corresponding absorbance values are given in Table3.1.

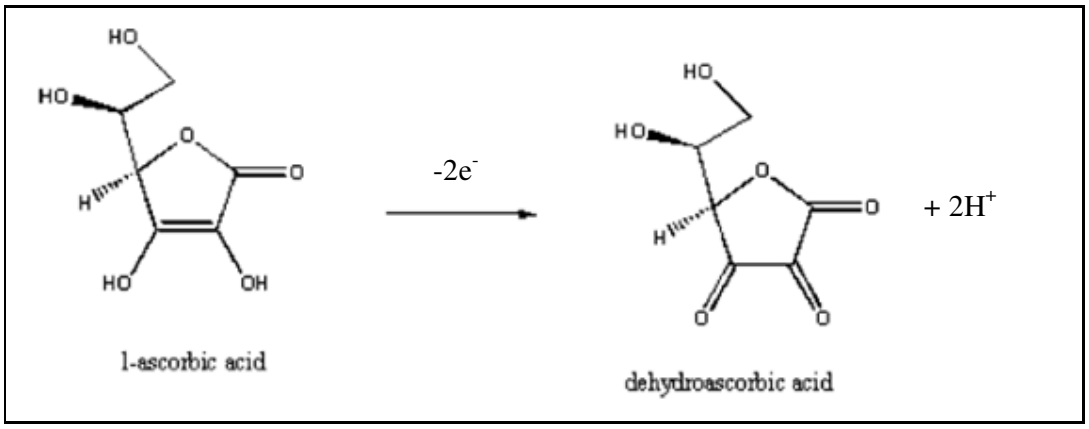

Figure 3.1 Schematic representation of oxidation of ascorbic acid to dihydroascorbate anion.

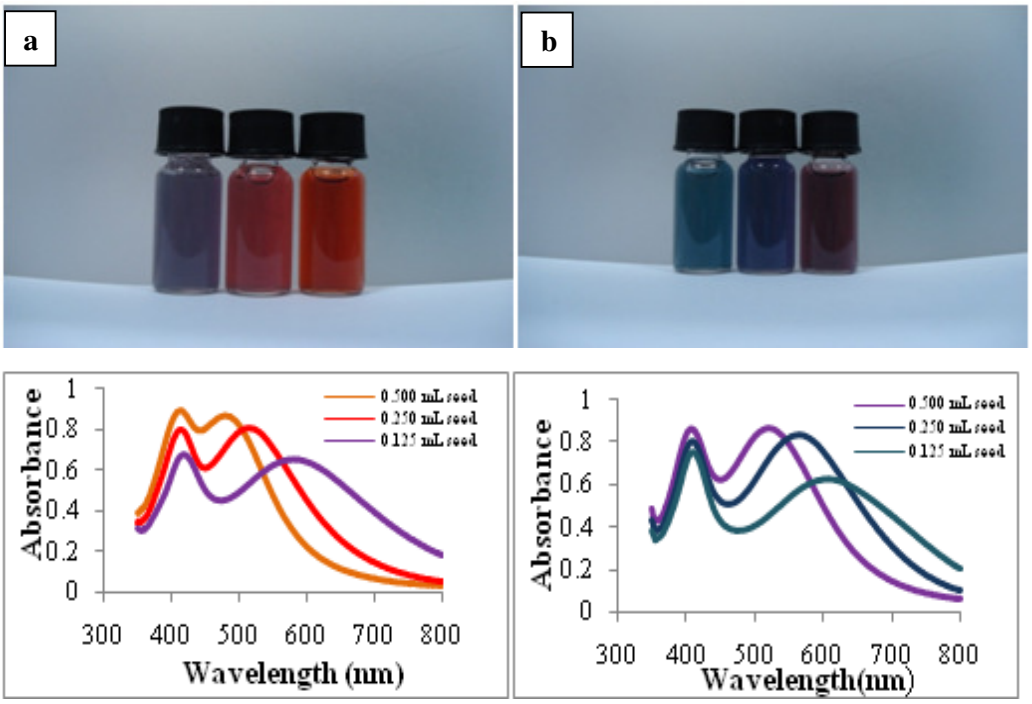

Figure 3.2 a) Growth solutions prepared with 0.018 M CTAB, 3.2×10^{-4} M $AgNO_3$, 2.1×10^{-3} M ascorbic acid, different volumes of seed (0.500, 0.250 and 0.125 mL) and 0.064 M NaOH **b)** Growth solutions prepared with 0.017 M CTAB, 3.1×10^{-4} M $AgNO_3$, 6.2×10^{-3} M ascorbic acid, different volumes of seed (0.5, 0.25 and 0.125mL) and 0.062 M NaOH

Table 3.1 The plasmon bands of growth solution of which absorption profile is given in Figure 3.6.

Concentration of ascorbic acid	**Volume of seed solution (mL)**		
	0.500	**0.250**	**0.125**
2.1×10^{-3} M	426 nm	415 nm	416 nm
	465 nm	499 nm	546 nm
6.2×10^{-3} M	410 nm	410 nm	410 nm
	502 nm	555 nm	602 nm

When the aspect ratio is increased the yellow color of the growth solution changes into blue and even blue- gray [48]. Moreover, the longitudinal plasmon band of the colloid shifts to red region of the spectrum. Thus, it can be stated that as the longitudinal plasmon band sifts to red region higher aspect ratio nanorods can be produced, Figure 3.2. Blue-gray corresponds to the largest red shift in the longitudinal plasmon absorption band (602 nm), Table 3.1. As can be seen from the Figure 3.2 and Table 3.1, ascorbic acid concentration of $6.2*10^{-3}$ M provides larger red shift (almost 50 nm) in the longitudinal plasmon band absorption at three different seed volumes compared to that of $2.1*10^{-3}$ M ascorbic acid. Thus the concentration of ascorbic acid in the growth solution was decided to be used as $6.2*10^{-3}$ M.

3.1.3.2 Ageing Time of Growth Solution

The nanorod formation starts as soon as the precursors of the growth solution were mixed. This was evidenced by a rapid color change from yellow to red, dark red, or green depending on the amount of seed used. The formation rate of the nanorods was also measured by monitoring the change in absorbance and the position of the silver plasmon band as a function of time. Although seven different sets of experiments were performed in which the volume of the seed added were varied, only the ones prepared by the addition of 0.250 mL and 0.125 mL seed solution gave both transverse and longitudinal surface plasmon bands that last during measurement period. Hence, these two sets were used for the determination of the aging time of growth solution. As can be seen from Table 3.2, as the solution ages the position of the longitudinal plasmon bands blue shifts whereas the transverse plasmon bands red shift slightly. The blue shift in the peak position of longitudinal plasmon band with time was associated with the change in aspect ratio of the developing rods. It is concluded that the aspect ratio of the rods increases quickly, and then slowly decreases over time. This observation agrees well with the previous studies [61]. Thus, it is decided to select 2 h as the aging time for the growth solution.

Table 3.2. The change in the wavelength and absorbance of the surface plasmon bands of growth solutions prepared with 0.250 mL and 0.125 mL seed addition with respect to time.

	0.250 mL seed		0.125 mL seed	
Time (h)	**Wavelength (nm)**	**Absorbance**	**Wavelength (nm)**	**Absorbance**
2	427	1.633	432	1.157
	580	1.490	621	0.833
4	423	1.629	430	1.170
	566	1.479	619	0.853
6	425	1.582	428	1.083
	548	1.452	593	0.753
21	431	1.403	431	0.892
	491	1.430	535	0.708
23	432	1.366	427	0.783
	483	1.407	524	0.603
25	435	1.336	427	0.798
	480	1.372	522	0.623

3.1.3.3 Seed Volume Optimization

In these studies almost 10 and 20 fold larger concentrations of ascorbic acid compared to that of silver nitrate were used. The colors of the growth solutions prepared at the stated conditions are also shown in Figure 3.2 together with their absorption spectra. The wavelengths of the longitudinal and transverse plasmon bands at their maximum and the corresponding absorbance values are given in Table 3.1.

We employed ascorbic acid as reducing agent of Ag^+ salts in the growth stage. The standard reduction potential for the Ag^+ (aqueous)/Ag_{metal} system is -0.80 V versus SHE. Ascorbic acid, being a weak reducing agent (reduction potential +0.275 V vs SHE), cannot reduce silver salt. Therefore, NaOH is added to the medium to increase the reduction power of the ascorbic acid. Besides, metallic seed must catalyze the reduction processes. Such catalytic reduction is due to particle mediated electron transfer from ascorbic acid to silver ions [62].

It has been stated that addition of silver nanoparticles as seeds has two advantages. Initially, it increases the overall reaction rate, and hence the growth rate; second, the particle size is controlled by varying the ratio of metal salt to seed, thus adjust the the particle size [55].

At two different volume of CTAB and at the same final concentration of silver salt, the volume of seed solution added to the growth solution was optimized**.** The change in the position and absorbance of the surface plasmon bands due to the change in the aspect ratio of the formed nanoparticles in the growth solutions were followed by UV-Vis spectrophotometer. The spectra obtained are given in Figure 3.3 and Figure 3.4 for following the surface plasmon resonance. The wavelengths of the longitudinal and transverse plasmon bands at their maximum and the corresponding absorbance values are given in Table 3.3 and Table 3.4.

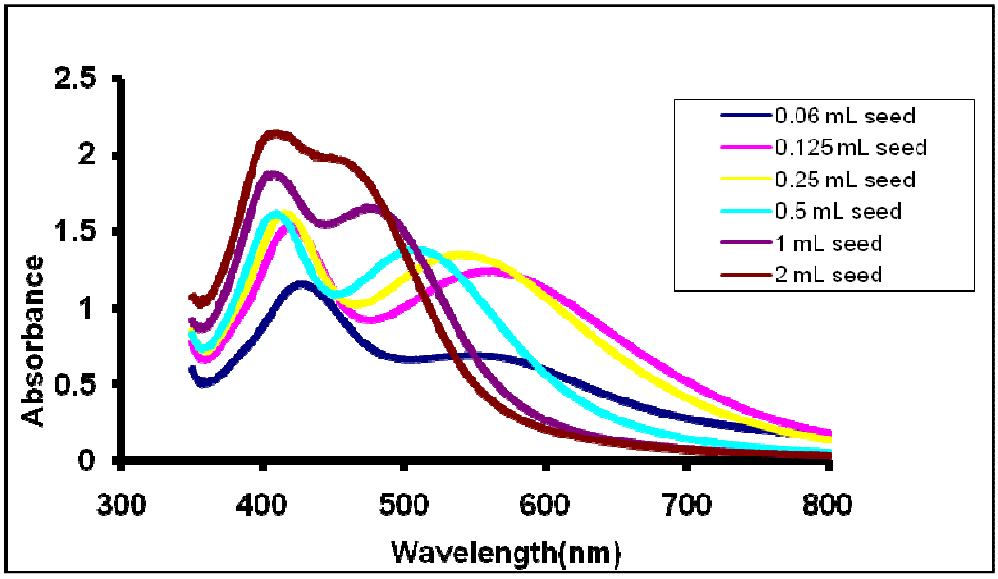

Figure 3.3 UV-visible absorption profile of growth solution prepared with 0.072 M CTAB, 2.25×10^{-4} M $AgNO_3$, 4.5×10^{-3} M ascorbic acid, different volumes of seed (2.00, 1.00, 0.500, 0.250, 0.125 and 0.060 mL) and 0.045 M NaOH.

Table 3.3 The plasmon bands of growth solution prepared with 0.072 M CTAB, 2.25×10^{-4} M $AgNO_3$, 4.50×10^{-3} M ascorbic acid, different volumes of seed (2.00, 1.00, 0.500, 0.250, 0.125 and 0.060 mL) and 0.045 M NaOH.

Volume(mL) of seed solution added	Peak maximum of Transverse Plasmon band	Absorbance value at the peak maximum	Peak maximum of Longitudinal Plasmon band	Absorbance value at the peak maximum e
0.060	425	1.154	-	-
0.125	418	1.533	555	1.241
0.250	411	1.600	534	1.346
0.500	407	1.609	506	1.381
1.00	403	1.879	470	1.644
2.00	404	2.143	448	1.989

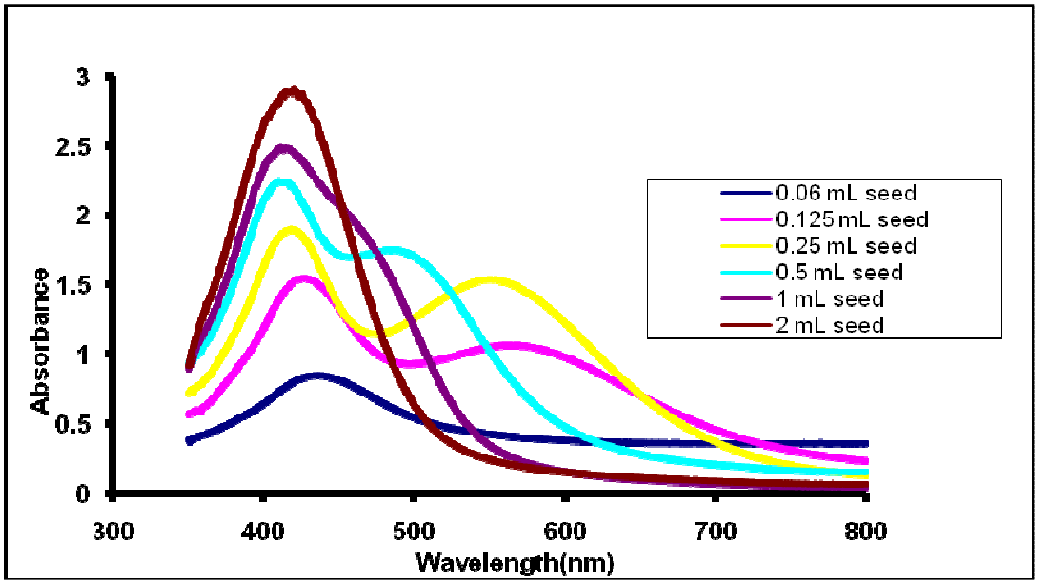

Figure 3.4 UV-visible absorption profile of growth solution prepared with 0.093 M CTAB, 2.58×10^{-4} M $AgNO_3$, 2.58×10^{-3} M ascorbic acid, different volumes of seed (2.00, 1.00, 0.500, 0.250, 0.125 and 0.06 mL) and 0.026 M NaOH.

Table 3.4 The plasmon bands of growth solution prepared with 0.093 M CTAB, 2.58×10^{-4} M $AgNO_3$, 2.58×10^{-3} M ascorbic acid, different volumes of seed (2.00, 1.00, 0.500, 0.250, 0.125 and 0.060 mL) and 0.026 M NaOH.

Volume(mL) of seed solution added	Peak maximum of Transverse Plasmon band	Absorbance value at the peak maximum	Peak maximum of Longitudinal Plasmon band	Absorbance value at the peak maximum
0.060	434	0.848	-	-
0.125	422	1.538	562	1.064
0.250	416	1.896	553	1.504
0.500	410	2.247	485	1.752
1.00	409	2.47	-	-
2.00	418	2.896	-	-

As it can be seen from the absorption profiles of growth solutions, Figure 3.3 and Figure 3.4, seed volume of 0.250 mL provide the appearance of both transverse and longitudinal surface plasmon bands which were considered as the evidence of nanorod formation. Moreover, in most of the experiments the large red shift of the longitudinal mode, indicating the formation of high aspect ratio nanorods and high absorbance value indicating the yield, are achieved by the same amount of seed. To be able to see both transverse and longitudinal mode in a good yield, it is decided to use 0.250 mL seed for the preparation of growth solution.

An increase in the seed volume (1.00 mL, 2.00 mL), for the same concentration of silver(I) ions, causes a big blue shift and even the disappearance of the longitudinal plasmon band, Figure 3.3 and Figure 3.4. This fact can be explained by the presence of small amount of Ag^+ ions available per seed particle in the growth solution. Therefore, it is normal to expect a decrease in the rod length, and probably formation

of very short rods with a small number of spheres. At very low volume of the seed (0.060 mL), on the other hand, due to the short of nucleation centers for the further growth of the particles for nanorod formation, the longitudinal plasmon band fades away, Figure 3.3 and Figure 3.4.

3.1.3.4 CTAB Optimization

Surfactant used in the growth solution is composed of trimethyl ammonium bromide head group and an alkyl chain. The general formula of the surfactant is given as C_nTAB where n changes as 10 (decyl), 12 (dodecyl), 14 (myristyl), and 16 (cetyl). The critical micelle concentration of C_nTAB in aqueous solution decreases logarithmically with the carbon number in the tail (from mM for n= 10 to 10 μM for n= 16). The general trend is that, as the length of the alkyl chain is increased, higher-aspect ratio nanorods can be obtained [63]. Therefore, in these studies the surfactant having the largest carbon number, cetyltrimethylammonium bromide (C_{16}TAB) was used as a stabilizing agent and a directing agent for silver nanorod synthesis.

The rod directing properties of C_{16}TAB was explained through its adsorption behavior. El-Sayed and co-workers [64] have suggested that the CTAB binding takes place via the metal-Br-surfactant complex formation. They have stated that the bromide ion is the bridge between the metal surface having high electron density and the electron deficient quaternary nitrogen of the headgroups [64]. C_{16}TAB forms bilayers on silver nanorods, with the positively charged trimethylammonium bromide headgroup of one monolayer facing the silver surface and the other facing the solvent to maintain water solubility [65] The large headgroup size of the C_{16}TAB surfactant preferred the larger metal-atom spacing on the sides rather than at the ends of the nanorods [66]. As shown in Figure 3.5, van der Waals interactions among interchain packing assists the underlying nanorod formation [63].

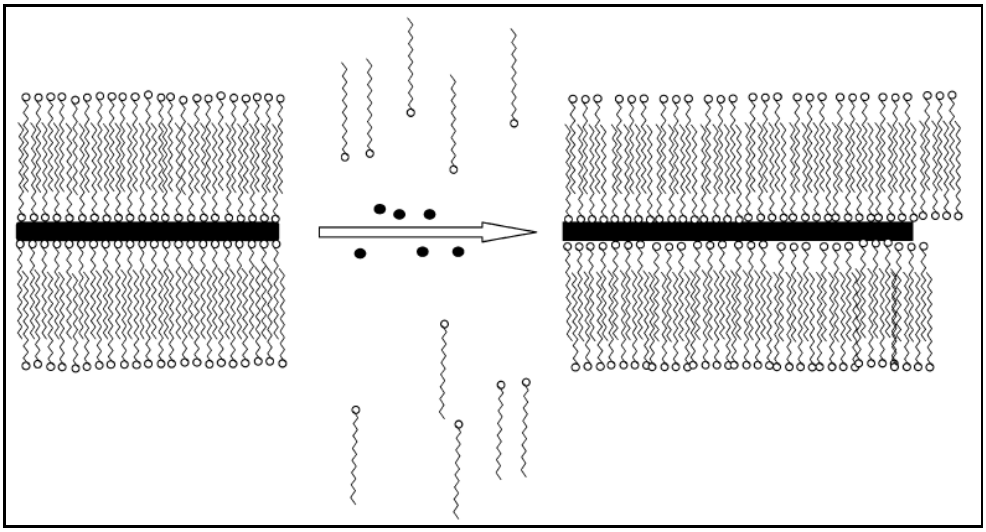

Figure 3.5 Cartoon illustrating the formation of the bilayer of C_nTAB (squiggles) on the nanorod (black rectangle) surface may assist nanorod formation as more metal ions (black dots) are introduced [63].

The effect of CTAB concentration on the aspect ratio of the nanorods formed were examined by altering the molarity of CTAB from 20 to 80 mM. The plasmon absorption spectra of the formed particles are presented in Figure 3.6. The wavelengths of the longitudinal and transverse plasmon bands at their maximum and the corresponding absorbance values are given in Table 3.5

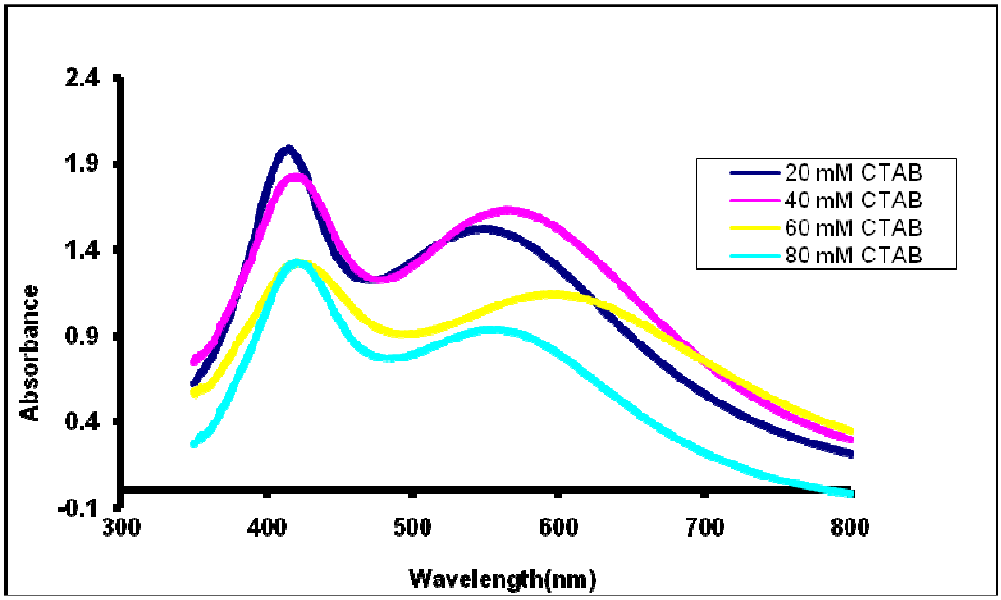

Figure 3.6 UV-visible absorption profile of growth solution prepared with 7 mL of different concentration of CTAB, $3.22*10^{-4}$ M $AgNO_3$, $2.06*10^{-3}$ M ascorbic acid, 0.250 mL seed, and 0.064 M NaOH.

Table 3.5 The plasmon bands of growth solution prepared with 7 mL different concentration of CTAB, $3.22x10^{-4}$ M $AgNO_3$, $2.06x10^{-3}$ M ascorbic acid, 0.250 mL seed, and 0.064 M NaOH.

Analytical concentration of CTAB in the final growth solution (mM)	**Peak maximum of Transverse Plasmon band (nm)**	**Absorbance value at the peak maximum**	**Peak maximum of Longitudinal Plasmon band (nm)**	**Absorbance value at the peak maximum**
20	413	1.978	549	1.522
40	416	1.820	564	1.639
60	418	1.312	594	1.141
80	418	1.322	552	0.934

As can be understood both from Figure 3.6 and Table 3.5, at all concentrations of CTAB the longitudinal and transverse plasmon bands are clearly observed. The maximum red shift in the position of the longitudinal plasmon band was obtained with a growth solution containing 60 mM concentration of CTAB. However, due to the difficulty of removing the adsorbed surfactant from the nanorods prepared, 20 mM CTAB concentration was preferred most of the time although it gives the lowest red shift among them. The optimized conditions for the growth solution are summarized in Table 3.6

Table 3.6 Optimized conditions for colloidal growth solution with the ageing time of 2 h.

Name of the reagent	**Added volume of the reagent (mL)**	**Molarity of the added reagent (M)**	**Analytical molar concentration of reagent in the final growth solution (M)**
CTAB	7.00	2.0×10^{-2}	1.70×10^{-2}
$AgNO_3$	0.250	1.0×10^{-2}	3.09×10^{-4}
Ascorbic acid	0.500	0.10	6.17×10^{-3}
Seed solution	0.250	-	**-**
NaOH	0.100	5.00	6.17×10^{-2}

The volume of the growth solution is mainly determined by the volume of the CTAB solution. The contributions of the other reagents of the growth solution are negligible. Therefore, by changing the volume of the CTAB used in the growth only it was managed to re-examine the optimum concentrations of silver nitrate and ascorbic acid solutions. $AgNO_3$ concentration was varied from 4.34×10^{-4} M to 2.32×10^{-4} M. and ascorbic acid concentration was varied from 8.68×10^{-3} M to 4.64×10^{-3} M as can be followed from Table 3.7. The spectra obtained are given in Figure 3.7.

The wavelengths of the longitudinal and transverse plasmon bands at their maximum and the corresponding absorbance values are given in Table 3.7

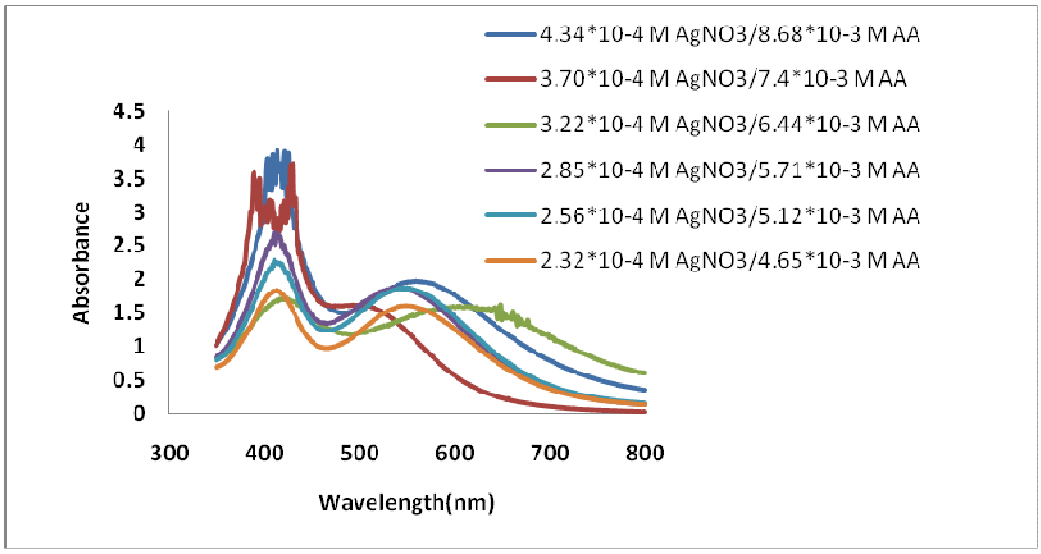

Figure 3.7 UV-visible absorption profile of growth solution prepared with 80 mM different volumes of CTAB (5.00 mL,6.00 mL, 7.00 mL, 8.00 mL, 9.00 mL, 10.00 mL) 0.25 mL 10 mM $AgNO_3$, 0.25 mL seed and 0.10 mL 5 M NaOH. AA: ascorbic acid

Table 3.7 The plasmon bands of growth solution prepared with different volumes of 80 mM CTAB (5.00 mL,6.00 mL, 7.00 mL, 8.00 mL, 9.00 mL, 10.00 mL), 0.25 mL of 10 mM $AgNO_3$, 0.25 mL seed and 0.1 mL of 5 M NaOH

Analytical molar concentration of $AgNO_3$ in the final growth solution (M)	**Analytical molar concentration of ascorbic acid in the final growth solution (M)**	**Peak maximum of Transverse Plasmon band (nm)**	**Absorbance value at the peak maximum**	**Peak maximum of Longitudinal Plasmon band (nm)**	**Absorbance value at the peak maximum**	**Volume of CTAB (mL)**
$4.34x10^{-4}$	$8.68x10^{-3}$	417	3.727	563	1.969	5
$3.70x10^{-4}$	$7.4x10^{-3}$	415	2.899	507	1.605	6
$3.22x10^{-4}$	$6.44x10^{-3}$	425	1.707	612	1.588	7
$2.85x10^{-4}$	$5.71x10^{-3}$	416	2.653	548	1.855	8
$2.56x10^{-4}$	$5.12x10^{-3}$	417	2.243	550	1.865	9
$2.32x10^{-4}$	$4.65x10^{-3}$	416	1.819	550	1.596	10

As can be seen from Figure 3.7 and Table 3.7, the best results-in terms of shift of the longitudinal plasmon band and the absorbance value of that band indicating the yield were obtained when the growth solution as prepared with $3.22*10^{-4}$ M $AgNO_3$ and $6.44*10^{-3}$ M ascorbic acid. These values were all in accordance with the optimized values so far, Table 3.6.

3.1.3.5 Repeatability of the Optimized Growth Conditions

After optimizing the conditions, all experiments throughout the study were performed three times in the same day. The repeatability of the experiments were very close to each other when they were followed by UV-visible spectrometer. In Figure 3.8, it is obvious that both the transverse and longitudinal plasmons were very close to each other in terms of position and peak maximum of bands.

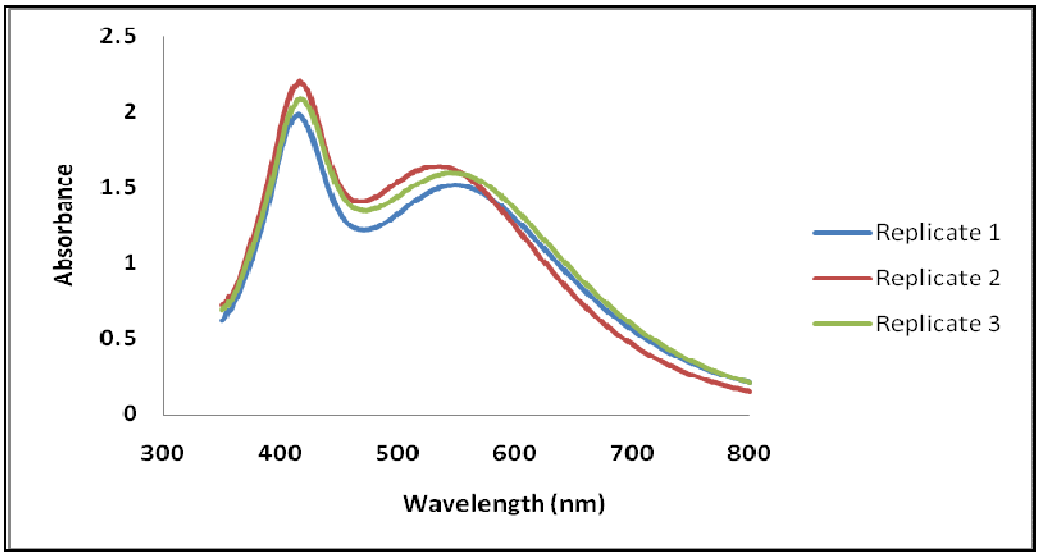

Figure 3.8 The growth solutions prepared in the same way in the same day. The solution containes $1.8*10^{-2}$ M CTAB, $3.22*10^{-4}$ M $AgNO_3$, $2.06*10^{-3}$ M ascorbic acid, 0.250 mL seed, $6.4*10^{-2}$ M NaOH.

3.1.3.6 Sequence of Addition of Reagents to the Growth Solution

In our general synthesis, the template which is $C_{16}TAB$ was prepared by heating to prevent precipitation. After that $AgNO_3$, ascorbic acid, seed and NaOH were added, respectively. As stated before to see the longitudinal plasmon band as well as transverse plasmon band 0.100 mL of 5 M NaOH which is 5 times more in terms of concentration than the value stated in literature was added [46,47]. However, when

the solid $AgNO_3$ is dissolved with CTAB in deionized water, 0.1 mL of 1 M NaOH was sufficient to see the separation of plasmon bands in the presence of all different volumes of seed.

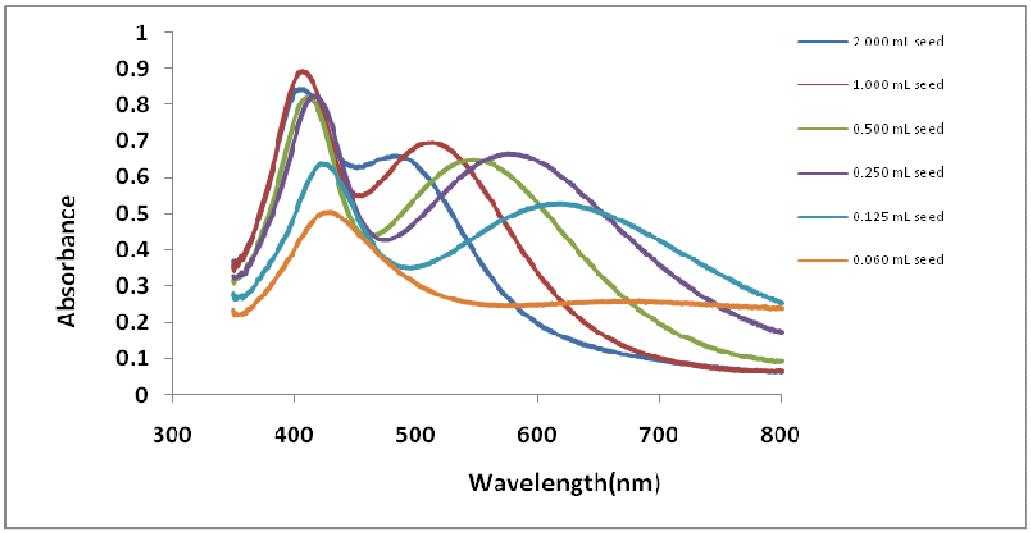

Figure 3.9 UV-visible absorption profile of growth solution prepared with "stock growth solution" with 0.1 mL of 1 M NaOH solution.

3.2 Characterization of Nanoparticles

After UV–vis measurement the growth solution prepared with 0.125 mL seed as in 2.3.1.2.7 in experimental part, solution was centrifuged at 5000 rpm in order to separate rods and spheroids from the silver nanoparticles present in the solution. The centrifugate was washed three times with distilled water and its FE-SEM image was taken in METU Central Laboratory (Figure 3.10).

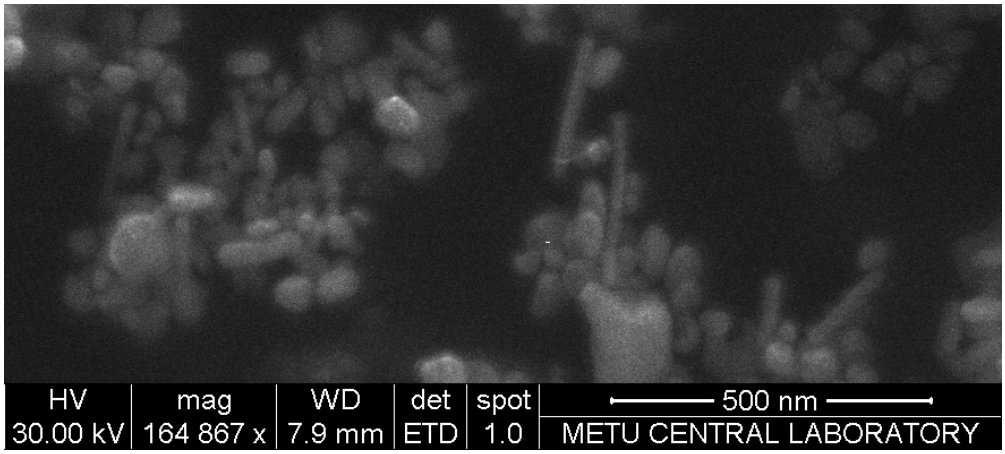

Figure 3.10 The field emission-scanning electron microscopy image of the nanostructures prepared by the growth solution containing 0.12 mL seed solution

As can be seen from the figure, the centrifugate is consisting of long and short nanorods and spheroids. The aspect ratio of the spheroids is around 2–4. The mean length of thus prepared short silver nanorods is in the range of 70–80 nm and their aspect ratios are about 4–5. The mean aspect ratio of the long ones is about 12. The shapes of nanorods are clearly distinguishable from the spheroidal shape.

3.3 Preparation and SERS characterization of glass substrates through seed-mediated growth approach

For the coverage of the glass surfaces with silver nanorods through seed-mediated growth technique, the glass plate was simply immersed into the seed solution and then into the growth solution. The coated glasses were used as SERS substrates and the performances of coatings were evaluated in terms of their SERS activity. Brilliant cresyl blue (BCB) and crystal violet (CV) were used as model compounds. Besides the SERS detection of benzoic acid (BA), a commonly used food preservative, was investigated.

3.3.1 Parameters affecting SERS intensity of nanoparticles attached to the sol-gel coated glass substrate

The conditions optimized for the preparation of nanorods in the solution phase were adapted to the preparation of solid substrates. However, to enhance the SERS signal, the possible effects of some modifications such as the increase of $AgNO_3$ concentration in the growth solution and the addition of hydrocarbons to the growth solution were examined.

The crucial role of seeds in the seed-mediated growth approach of silver nanorods is well known [55,67]. Therefore, the efficient seeding of the surface is one of the critical point for coating the surface with nanostructures. At the beginning, it was attempted to activate the glass surfaces by soaking them in acidic solutions (acetic acid, nitric acid and piranha solution which is a typical mixture is 3:1 concentrated sulfuric acid to 30% hydrogen peroxide solution [67] prior to the seeding step. After the seeding and growth processes, the nanostructure covered glasses were used as a SERS substrate for the collection of BA spectrum. Only few of these substrates were SERS active, most of them did not give any SERS signal for 1.0×10^{-2} M BA.

The seed mediated growth technique has been used for the preparation of Indium Tin Oxide (ITO) electrode surfaces [68,69]. They have also given emphasis to the importance of surface roughness for the adsorption of gold nanostructures on the ITO surface [69]. Hence in order to provide the roughness on the glass surface it is decided to use glass plates coated with a thin film of sol-gel. This porous, highly hydroxylated, surface worked very well for attaching silver seeds on the surface. Throughout this text whenever glass substrate is stated it corresponds to *sol-gel coated glass*.

Besides the amount of seed in the medium, the ratio of seed content to $AgNO_3$ concentration is also a very important parameter [46]. In the application of seed mediated growth technique for the preparation of silver nanorods on the surface of glass, it is not possible to predict the seed quantity introduced on to the surface. Therefore, the concentration of silver nitrate, ascorbic acid and CTAB were increased 3 and 5 fold of the optimized growth solution. The pH of the solutions was adjusted to 11 by the addition of 5.0 M NaOH. The SERS performances of the substrates prepared at these high concentrations of silver in the growth solution were evaluated by using $1.0x10^{-6}$ M BCB. For the Raman spectrum of brilliant cresyl blue, the intense band at 580 cm^{-1} is assigned to the benzene ring deformation mode [70].

3.3.1.1 Effect of silver nitrate

To observe the effect of $AgNO_3$, its concentration in growth solution was increased to 3 and 5 times from the original amount. The performance of the nanoparticle attached solid substrate was examined with 10^{-6} M BCB in Raman spectroscopy. As can be seen from Figure 3.10 ther,e is a substantial increase in the signal (ca. 30 fold) when 5 fold concentration of Ag^+ relative to the growth solution was used.

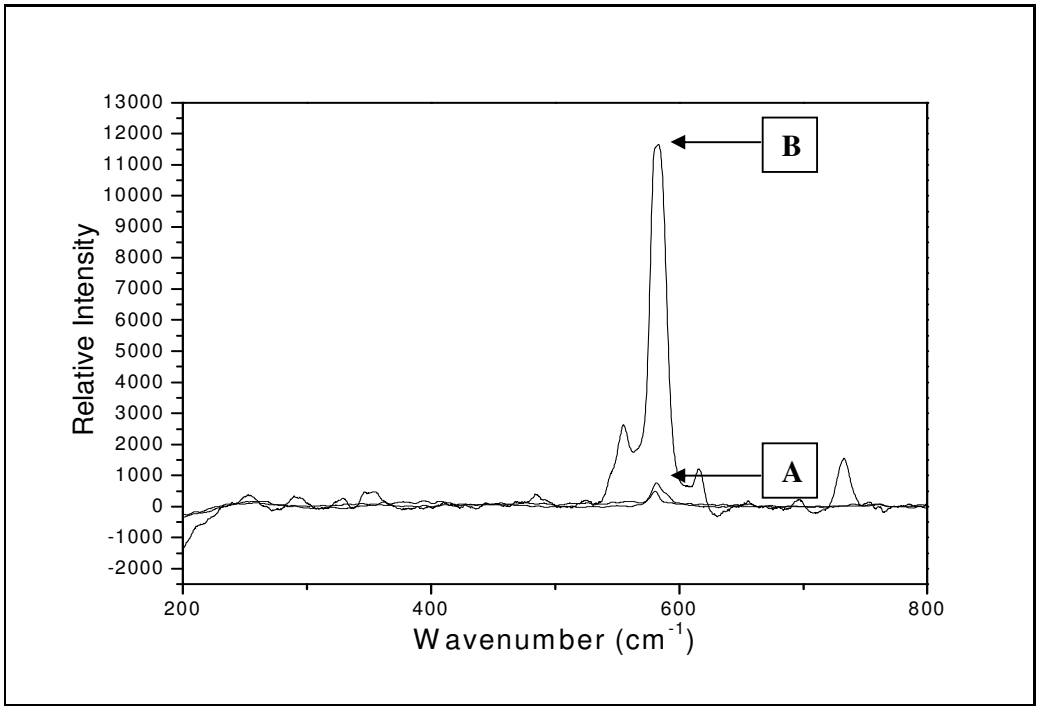

Figure 3.11 .The variation of the relative SERS intensities of 10^{-6} M BCB collected on the solid substrates prepared by (A) 3 and (B) 5 fold greater Ag^{+} concentration than the optimized growth solution

3.3.1.2 Effect of organic hydrocarbons to the growth solution to prepare nanoparticle attached solid substrate

The effects of polar and nonpolar molecules on the average shape and aggregation number of surfactants are well known. It has been stated that the presence of polar substances and small amounts of some aliphatic hydrocarbons such as cyclohexane, n-dodecane in the solution of cationic surfactants cause the formation of rod type micelles [71]. The elongation effect of cyclohexane addition for the gold nanorods was investigated by Murphy's group [8]**.**

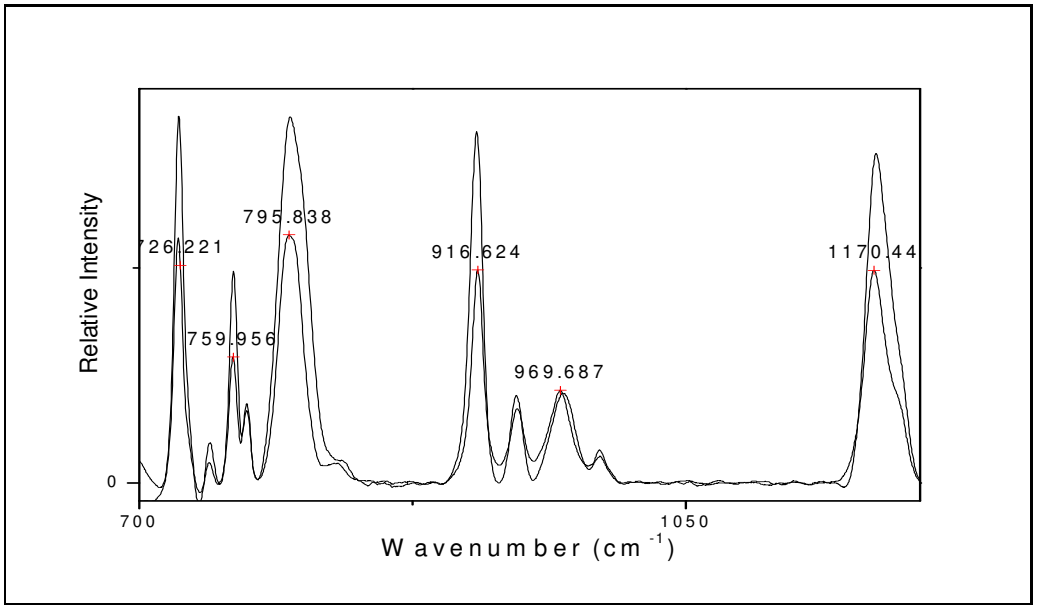

Figure 3.12 The variation of the relative SERS intensities of 1.0×10^{-6} M CV collected on the solid substrates prepared by growth solution in the absence (lower trace) and in the presence (upper trace) of 0.36 mL of pure acetone**.**

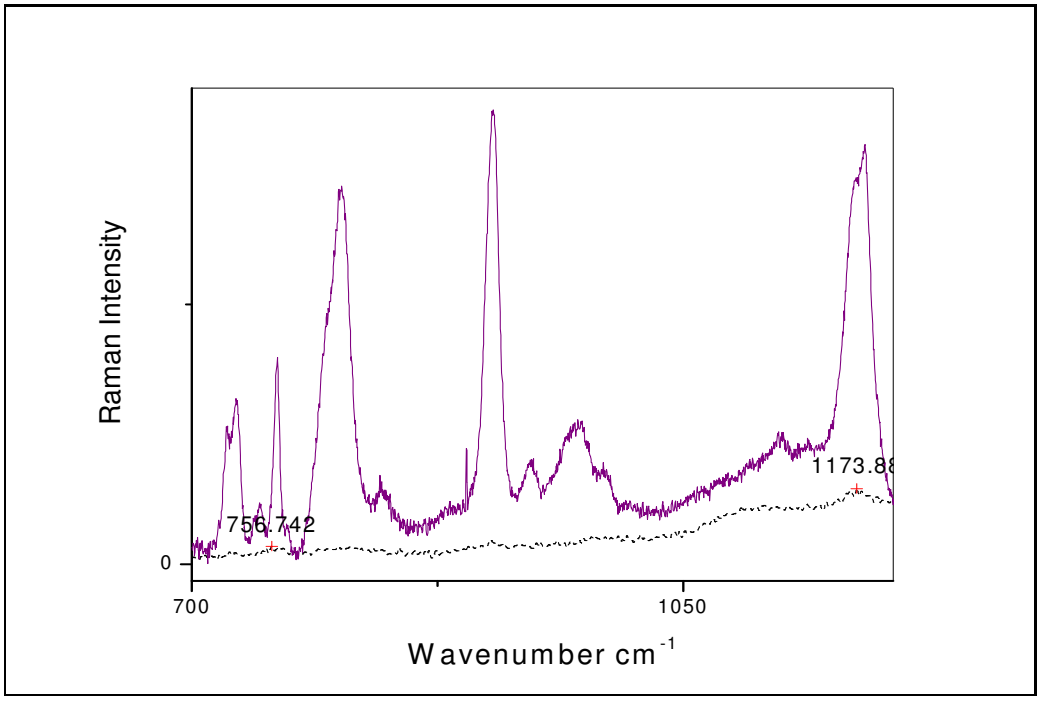

Figure 3.13. The variation of the relative SERS intensities of $1.0x10^{-6}$ M CV collected on the solid substrates prepared by growth solution in the absence (lower trace) and in the presence (upper trace) of 0.27 mL cyclohexane.

According to the literature [72] in the Raman spectrum of CV, C-H out-of-plane bendings are observed at about 726, 759 and 795 cm^{-1}, whereas ring skeletal vibrations appear at about 922 cm^{-1} and 953 cm^{-1}. The band at 1170 cm^{-1} is attributed to C-H in-plane bending vibrations. For the Raman spectrum of BCB, the intense band at 580 cm^{-1} is assigned to the benzene ring deformation mode [73]. As can be seen from Figure 3.12 and Figure 3.13, by the addition of either acetone or cyclohexane SERS signals were increased. The enlargement is larger in the case of cyclohexane addition. However, in their presence background signal became complicated due to the appearance of several new features. Therefore we decided to discard the addition of cyclohexane and acetone to the medium.

3.3.1.3 Effect of seed addition to the growth solution to prepare nanoparticle in colloid

The electrical field enhancement of the silver nanorods prepared on Raman signal was investigated by acquiring the SERS spectra of 10^{-2} M BA solution with the nanorod colloid solutions, Figure 3.14. According to the literature, the peak at 998 cm^{-1} corresponds to the benzene ring breathing of BA [74]. Therefore, the intense peak observed at 1002.5 cm^{-1} was assigned to the breathing motion of the benzene ring.

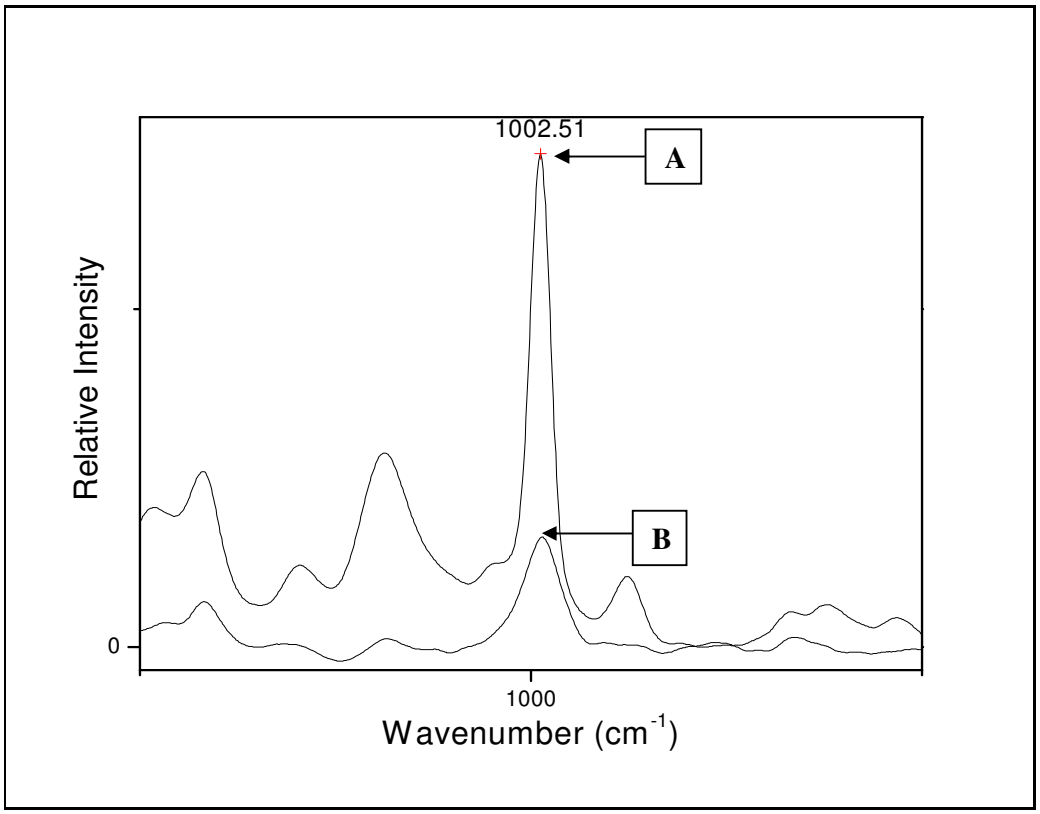

Figure 3.14 The variation of the relative SERS intensities of BA (10^{-2} M) collected with growth solutions prepared by (A) the addition of 0.125 mL seed solution; (B) the addition of 0.25 mL seed solution.

As can be seen from the Figure 3.14, there is a 4 fold increase in the SERS signal of BA collected in the growth solution (A) (prepared by 0.125 mL seed solution) compared to that of (B) (prepared by 0.250 mL seed solution). As expected nanorod solution having a plasmon absorption wavelength similar or even longer than the emission wavelength of He-Ne laser which is 632.8 nm, (A) in Figure 3.14, was provided the stronger electromagnetic enhancement.

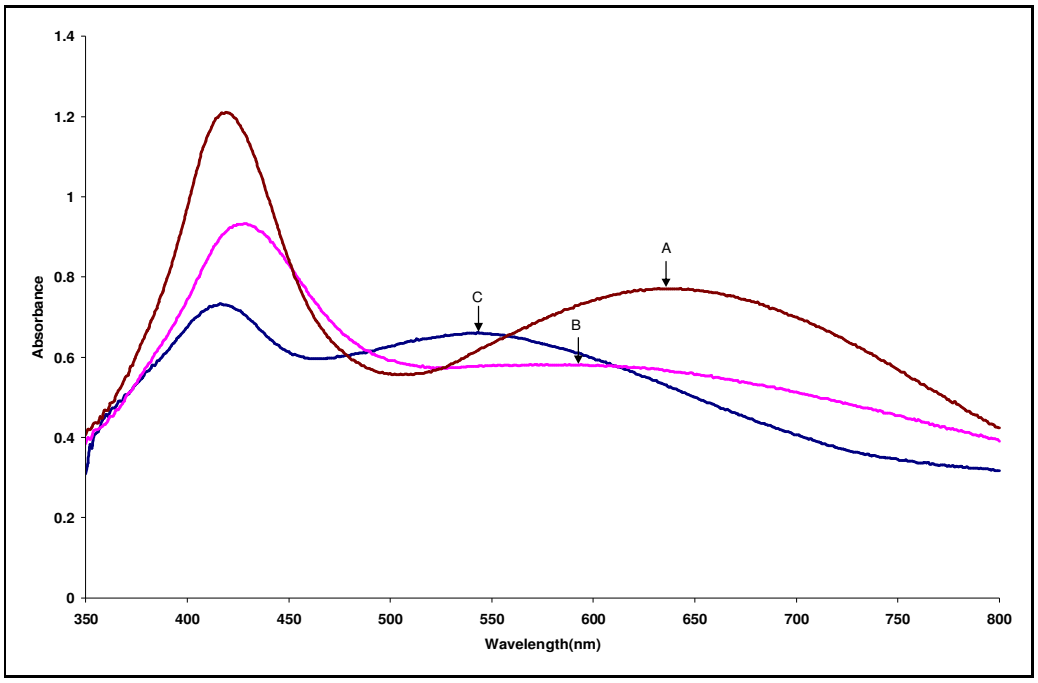

Figure 3.15 The UV-VIS spectra of silver nanorod colloids prepared by (A) the addition of 0.125 mL seed solution ; (B) the addition of 0.25 mL seed solution ; (C) the addition of 0.5 mL seed solution to the growth solutions.

3.3.1.4 SERS performance of nanoparticle colloid vs SERS performance of nanoparticle attached solid substrate

The SERS spectra of 10^{-2} M BA acquired with the silver nanorods colloid solution and silver nanorod coated solid substrate, both prepared through seed mediated growth technique, were compared.

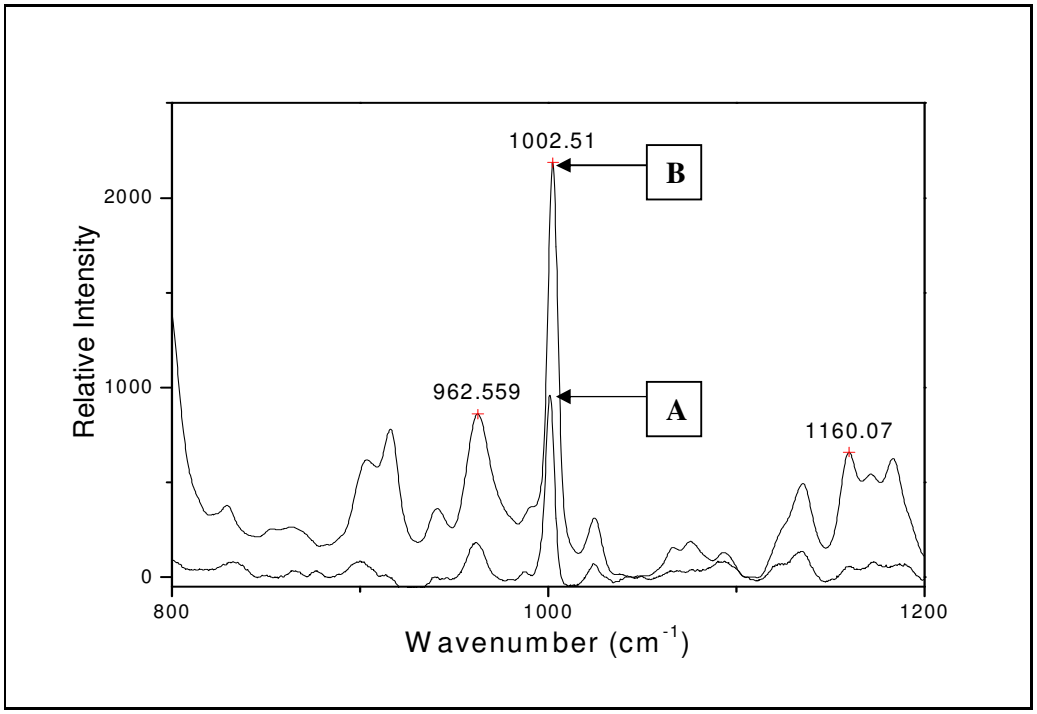

Figure 3.16 The SERS spectra of 10^{-2} M BA acquired with the silver nanorods colloid solution (A) and silver nanorod coated solid substrate (B).

As can be seen from Figure 3.16, there is only 2 fold decrease in the signal when the solid substrate was used. It is known that [75] the SERS sensitivity of colloidal substrates are generally higher than film type substrates.

CHAPTER 4

CONCLUSIONS

We managed to produce silver nanorods and nanospheroids using seed mediated growth approach. The Ag seeds, were prepared by chemical reduction of $AgNO_3$ by $NaBH_4$ in the presence of trisodium citrate to stabilize the nanoparticles. To make nanorods, $AgNO_3$ was reduced by ascorbic acid in the presence of seed, the micellar template cetyltrimethylammonium bromide (CTAB), and NaOH. The pH of the growth solution, the seed, C_{16}TAB and silver nitrate concentrations were critical an they were optimized thoroughly. The electronic absorption spectra of silver nanorod solutions show the conventional 400 nm peak observed for spherical silver seeds and another peak at longer wavelengths, due to the longitudinal plasmon band of rod-shaped particles. The appearance of the second peak and its position in wavelength scale were followed by a UV-vis spectrophotometer as an indication of rod formation. Our optical data were in accord with what others have observed for metallic nanorods for transverse and longitudinal plasmon bands. Rods and spheroids can be separated from spheres by centrifugation. For the characterization of the nanoparticles formed FESEM was used. According to the FESEM measurement, the aspect ratio of the spheroids was around 2–4. The mean length of thus prepared short silver nanorods was in the range of 70–80 nm and their aspect ratios were about 4–5. Whereas, the mean aspect ratio of the long ones was about 12. The prepared colloidal nanorod solutions were used as a SERS active medium.

Due to their unique and tunable optical properties silver and gold nanorods attract considerable attention as an active medium for the development of sensitive chemical and biological SERS sensors. Practical application of SERS requires the transfer of these nanorods onto the surface of a solid substrate without disturbing their surface

plasmon properties. Usually nanorods are prepared in the solution, then they are attached on the surface of the substrate via a linker molecule. This is the first time that the nanorods growth on the surface is used as a SERS substrate. The intense spectra obtained for brilliant cresyl blue, crystal violet and benzoic acid, demonstrated the efficiency of the prepared substrate for the SERS enhancement and its potential as a SERS detection probe for chemical and biological analysis. The shelf life of the solid SERS substrate is more than one month. Current efforts are being devoted towards extending the usefulness and applicability of this new SERS-active solid substrate.

REFERENCES

1 Skoog,D.A; Holler,F.J.; Nieman, T.A; *Principles of Instrumental Analysis;* 5th edition; Saunders College Publishing; Philadelphia; **1997**; pp 429-432.

2 Strobel, H.A.;Heineman, R.W; *Chemical Instrumentation: A systematic approach*; 3rd edition; John Wiley & Sons; New York; **1989**; pp: 633-636.

3 Willard,H.H.; Merritt, L. L.; Dean, J. A.; Settle, F. A.; *Instrumental Methods of Analysis*; 7th Edition; Wadsworth Publishing Company; **1988**; pp.321-325

4 Kneipp,K.; Kneipp, H. ; Itzkan, I. ; Dasari, R. R. ; Feld, M. S. ; *J.Phys.:Condens.Matter*, **2002** 14, R597

5 Shony,R-S., Zhu, L. and Morris, M.D.; *Anal.Chem.*, **1988** 58, 1116,.

6 Ritchie, R.H.; *Phys. Rev*. **1957** 106, 879.

7 L. Li, J. Hu, W. Yang, A. P. Alivisatos, *NanoLetters* **2001** 1, 349.

8 El-Sayed, M.A.; *Accounts of Chemical Research* **2001** 34,4,257

9 Creighton, J A.; Eadon D G; *J. Chem. Soc. Faraday Trans.* **1991** 87, 3881

10 Mie, G;. *Ann. Phys*.**1908** 25, 329.

11 Mulvaney, P.;. *Langmuir* **1996** 12, 788

12 Gans, R. *Ann. Phys*. **1912** *37*, 881

13 Foss, C. A.; Hornyak, G. L.; Stockert, J. A.; Martin, C. R. *J. Phys. Chem*. **1994**, *98*, 2963

14 Lebedeva, V. N.; Distler, G. I. *Opt. Spectrosc*. **1967** *23*, 527

15 Blatchford, C. G.; Campbell, J. R.; Creighton, J. A. *Surf. Sci*. **1982** *120*, 435

16 van der Zande, B. M. I.; Böhmer, M. R.; Fokkink, L. G. J.;Schönenberger, C. *J. Phys. Chem. B* **1997** 101, 852.

17 Haes, A. J.; Zou,S.; Schatz,G. C.; Van Duyne,R. P.; *J. Phys. Chem. B* **2004** 108, 109.

18 Nie, S.; Emory,S. R.; *Science* **1997** 275, 1102.

19 Barnes, W. L., Dereux, A.; Ebbesen, T.W.; *Nature* **2003** 424, 824.

20 Maier, S. A.; Kik,P. G.; Atwater, H. A.; Meltzer, S.; Harel,E.; Koel, B.E.; Requicha, A.A.G;. *Nat.Mater*. **2003** 2, 229.

21 Oleg, P.; Varnavski, M. B.; Mohamed, A. M.; Mostafa,A. E.; Theodore, G.; *J. Phys. Chem. B* **2003** 107, 3101.

22 Rechberger, W.; Hohenau, A.; Leitner, A.; Krenn, J. R.; Lamprecht, B.; Aussenegg, F. R.;*Opt.Commun*. **2003** 220, 137

23 Mock, J. J.; Oldenburg, S. J.; Smith, D. R.;Schultz, D. A.;and S. Schultz, *Nano. Lett.* **2002** 2, 465.

24 Lal, S.; Taylor, R. N.; Jackson, J. B.; Nordlander, P.; Halas, N. J.; *J. Phys. Chem. B* **2002** 106, 5609.

25 Colleen, L. N.;Nathaniel, K. G.; Glenn, P. G.; Felicia,T.; Naomi, J. H.; Jason, H. H *Nano. Lett* **2004** 4, 2355.

26 Link,S; El-Sayed, M. A.; *J.Phys.Chem.B* **1999** 103, 8410.

27 Sun, Y.; Xia, Y; *Adv.Mater* **2002** 14, 833.

28 Hirai, H.; Wakabayashi, H.; Komiyama, M.; *Chem. Lett.* **1983** 1047.

29 Brugger, P.-A.; Cuendet, P.; Gratzel, M.. *J. Am. Chem. Soc.* **1981** *103*, 2923

30 Thomas, J. M.; *Pure Appl. Chem.* **1988** *60*, 1517.

31 Charles, S. C.; Popplewell, J. *Ferromagnetic Materials*; **1980** 2, 154.

32 Schön, G.; Simon, U.; *Colloid Polym. Sci.* **1995** *273*, 202.

33 Whitney, T. M.; Jiang, J. S.; Searson, P. C.; Chien, C. L. *Science* **1993** *261*, 1316.

34 Tsuya, N.; Tokushima, T.; Shiraki, M.; Wakui, Y.; Saito, Y.; Nakamura, H.; Harada, Y. *IEEE Trans. Magn.* **1988** 24, 2661.

35 Tsuya, N.; Tokushima, T.; Shiraki, M.; Wakui, Y.; Saito, Y.; Nakumara, H.; Katsumata, Y. *IEEE Trans. Magn.* **1987** 23, 53.

36 Shiraki, M.; Wakui, Y.; Tokushima, T.; Tsuya, N. *IEEE Trans. Magn.* **1985** 21, 1465.

37 Arai, K. I.; Kang, H. W.; Ishiyama, K. *IEEE Trans. Magn.* **1991** 27, 4906.-

38 Martin, C. R. *Science* **1994** 266, 1961

39 Foss, C. A.; Tierney, M. J.; Martin, C. R. *J. Phys. Chem.* **1992** 96, 9001.

40 Al-Rawadesh, N. A. F.; Sandrock, M. L.; Seugling, C. J.; Foss, C. A., Jr. *J. Phys. Chem. B* **1998** 102, 361.

41 Hulteen, J. C.; Martin, C. R. *J. Mater. Chem.* **1997** 7, 1075

42 Yu,Y. Y.; Chang, S. S.; Lee, C. L.; Wang, C. R. C.; *J. Phys. Chem. B* **1997** 101, 6661.

43 Link, S.; Mohamed, M. B.; El-Sayed, M. A.; *J. Phys. Chem. B* **1999** 103, 3073.

44 Pileni, M. P.; Ninham, B. W.; Gulik-Kryzwicki, T., Tanori, J.; Lisiecki, I.; Filankembo, A.; *Adv. Mater*. **1999** 11, 1358.

45 Peng, X. G.; Manna, L.; Yang, W. D.; Wickham,J; Scher, E.; Kadavanich, A; Alivisatos, A.P.; *Nature* **2000** 59, 404,

46 Filankembo,A.; Pileni, M.P.; *J. Phys. Chem. B* **2000** 104, 5865.

47 Li. M.; Schnablegger, H.; Mann, S.; *Nature* **1999** 402, 393.

48 Jana,N. R.; Gearheart, L.;. Murphy, C. J.; *Chem. Commun*. **2001** 617.

49 Jana,N. R.; Gearheart, L.;. Murphy, C. J.; *J. Phys. Chem. B* **2001** 105, 4065.

50 Orendorff,C.J;Gearheart, L.; Jana, N.R.;Murphy,C.J; *Phys.Chem.Chem.Phys* **2006** 8, 165

51 Orendorff,C.J; Murphy,C.J; Sau,T.K.; *Small Communications* **2006** 5, 636.

52 Orendorff,C.J; Murphy,C.J.; Baxter, S.C.; Goldsmith, E.C.; *Nanotechnology* **2005** 16, 2601.

53 Orendorff,C.J; Murphy,C.J.; Gole, A.; *Langmuir* **2004** 20, 7117.

54 Orendorff,C.J; Murphy,C.J.;Hankins, P.L.; *Langmuir* **2005** 21, 2022.

55 Orendorff,C.J; Murphy,C.J.; Jana, N.R.; *J.Phys.Chem.B* **2001** 105,4065.

56 Busbee, B.D.;Obare, S.O.; Murphy, C.J.; *Adv.Mater* **2003** 15,414.

57 Orendorff,C.J; Murphy,C.J.; Jana, N.R.; *Adv.Mater* **2001** 13, 1389.

58 Murphy,C.J.; Jana, N.R.; *Adv.Mater* **2002** 14, 80.

59 Jiang, X.C.; Pileni, M.P.; *Colloids and Surfaces A: Physicochem. Eng. Aspects* **2007** 295, 228.

60 Chang, G.; Zhang, J.; Oyama, M.; Hirao, K.; *J. Phys. Chem., B*, **2005** 109, 1204.

61 Henglein, A.;Giersig, M.; *J.Phys.Chem B* **1999** 103, 9533.

62 Jana,N. R.; Gearheart, L.; Murphy, C. J.; *Chem. Commun.*, **2001** 617.

63 Jana,N. R.; Gearheart, L.; Murphy, C. J.; *Chem. Mater.* **2001** 13, 2313

64 Sau, T. K.;Murphy, C.J.; *Langmuir* **2004** 20, 6414.

65 Gole, A.; Orendorff, C. J.; Murphy, C. J.; *Langmuir* **2004** 20, 7117.

66 Pal,T.; De, S.; Jana, N. R.; Pradhan, N.; Mandal, R.; Pal, A.; Beezer, A. E.; Mitchell, J. C.; *Langmuir* **1998** 14, 4724

67 Gao, J.; Bender, C. M.; Murphy, C.J; *Langmuir* **2003** 19, 9065.

68 Germain, V.; Brioude, A.; Ingert, D.; Pileni; M. P.; *J. Chem. Phys*. **2005** 122 124707.

69 Busbee, B. D. ; Obare, S. O. ; Murphy, C. J. ; *Adv. Mater* **2003** 15, 414.

70 Chang,G.; Zhang, J.; Oyama, M.; Hirao, K.; *J. Phys. Chem., B* **2005** 109, 1204.

71 Umar, A.A; Oyama, M.; *Crystal Growth & Design* **2005** 5, 599.

72 Törnblom, M., Henriksson,U., *J. Phys. Chem., B* **1997** 101, 6028.

73 Jain, P.R.;Huang,X,;El-Sayed, I.H., El-sayed, M.A.; *Plasmonics* **2007** 2, 107.

74 Pe´rez-Juste, J.; Liz-Marza´n, L.; Carnie, M. S.; Chan,D. Y. C.; Mulvaney, P.; *Adv. Funct. Mater.*, **2004** 14, 571.

75 Kawabatal, S.; Ishikawa1, N.; Mitsui1, M.; Nakajima1,A.D.; *Eur. Phys. J.* **2007** 43, 155.

76 Orendorff,C.J; Gearheart, L.; Jana, N.R.; Murphy,C.J*; Phys.Chem.Chem.Phys* **2006** 8, 165.